Perspective

Antihydrogen chemistry

Mark C. Zammit,[1,*] Christopher J. Baker,[2,†] Svante Jonsell,[3,‡] Stefan Eriksson,[2,§] and Michael Charlton[2,‖]

[1]*Los Alamos National Laboratory, Los Alamos, New Mexico 87545, USA*

[2]*Department of Physics, Faculty of Science and Engineering, Swansea University, Singleton Park, Swansea SA2 8PP, United Kingdom*

[3]*Department of Physics, Stockholm University, SE-10691 Stockholm, Sweden*

(Received 8 November 2024; published 2 May 2025; corrected 7 May 2025)

A survey of antimatter reactions is presented, including the formation of the antihydrogen atom and anionic, cationic, and molecular species by collisional and radiative processes. Our approach is rooted in the detailed knowledge available for many matter counterpart (hydrogenic) reactions, due to their importance in controlling early Universe chemistry. We point out that the availability of trapped antihydrogen at densities similar to those pertaining to the epoch of hydrogen chemistry will soon be available. In addition, using modern atomic physics techniques, it should be feasible to control antimatter in the laboratory to facilitate antihydrogen chemistry. Our purpose is to summarize what is known from hydrogen chemistry that is of relevance for antimatter and to indicate, based on possible reaction rates, which processes may be fruitful to pursue to create new antimatter entities as probes of fundamental symmetries. We include antihydrogen, positrons, and antiprotons in our discussion and additionally the electron due to its propensity to form positronium and perhaps to participate in certain reactions. We attempt to indicate whether further theoretical/computational work is necessary to add to the assessment of reaction rates, and we discount processes where the projected rates are too low to be of interest, given foreseeable experimental capabilities.

DOI: 10.1103/PhysRevA.111.050101

I. INTRODUCTION

Recent years have seen dramatic advances in the production, trapping, and exploration of atomic antimatter in the form of antihydrogen, $\overline{\mathrm{H}}$, the positron- (e^+) antiproton ($\overline{p}$) bound state (see, e.g., Refs. [1–16]). In major further advances, the ALPHA Collaboration has achieved laser cooling of a trapped sample of the antiatoms and showed that spectroscopy with the cooled ensemble produces a narrower signal on the $1S$-$2S$ transition [17]. Very recently, the Collaboration reported on the observation of gravity on the motion of antihydrogen [18]. Many aspects of our discussion of antimatter chemistry are based on ALPHA's achievements, as this is currently the only antihydrogen collaboration able to trap and hold antiatoms for experimentation. Antihydrogen trapping is an enabler for many of the reactions we describe herein.

Antihydrogen is typically formed via the controlled mixing of e^+ and $\overline{p}$ clouds or plasmas in the presence of electric (of order 1–10 V cm^{-1}) and magnetic (in the tesla region) fields, and under the e^+ plasma conditions typically employed (with a characteristic temperature $T_e \sim$ 10–20 K, and a density, n_e, in the range 10^7–10^8 cm^{-3}) the antiatoms are created predominantly via the three-body reaction $e^+ + e^+ + \overline{p} \rightarrow e^+ + \overline{\mathrm{H}}$; See Sec. IV. Since the first formation of cold $\overline{\mathrm{H}}$ [2,3], this reaction has been studied extensively via simulation (see, e.g., Refs. [19–28]). It is well known that the process produces $\overline{\mathrm{H}}$ in highly excited states, with binding energies dependent on positron plasma parameters [29] in a subtle way, but typically of the order of a few 10s of $k_B T_e$, with k_B being Boltzmann's constant. The aforementioned experimentation with $\overline{\mathrm{H}}$ has been facilitated since the development of a magnetic minimum trapping apparatus for the antiatom [30], which allows the excited atoms to decay to the ground state and be stored and accumulated in an extreme high vacuum environment [4–8]. Some of the possibilities arising from these advances are discussed further in Sec. II.

The motivation for the detailed study of the properties of $\overline{\mathrm{H}}$ at low energies has recently been expounded in some detail in Refs. [31], which also contains a summary of the so-called Standard Model Extension (SME) formalism, as developed principally by Kostelecký and coworkers (e.g., Refs. [32,33]). The fundamental physics tests include exploration of CPT symmetry and the weak equivalence principle (WEP).

There has been substantial experimental progress in study of the $\overline{\mathrm{H}}$ $1S$-$2S$ transition hyperfine components [34] and ground-state hyperfine transitions, which offer complementary tests of CPT symmetry. The $1S$-$2S$ line is already determined for $\overline{\mathrm{H}}$ at a level better than a few parts in 10^{12} and will, with advances in laser and adiabatic cooling, hopefully soon approach the current precision of analogous

*Contact author: mzammit@lanl.gov
†Contact author: c.baker@swansea.ac.uk
‡Contact author: jonsell@fysik.su.se
§Contact author: s.j.eriksson@swansea.ac.uk
‖Contact author: m.charlton@swansea.ac.uk

measurements on ordinary hydrogen, which have a precision around 4×10^{-15} [35]. There is sensitivity to the WEP for antimatter via free-fall experimentation and clock measurements, and aspects of the interpretation of these tests were clarified in Ref. [31].

There is a thriving programme of antihydrogen and antiproton physics being undertaken at CERN's "Antimatter Factory": An excellent and accessible summary has been given recently by Carli *et al.* [36]. In addition to ALPHA, antihydrogen formation has also been achieved by the ASACUSA, AEgIS, and GBAR collaborations. ASACUSA has observed beamlike propagation of the antiatom [37] with the aim to perform an in-flight measurement of its hyperfine splitting [38]. AEgIS and GBAR intend to perform investigations of the gravitational behavior of antihydrogen and both have reported antiatom formation using the antiproton-positronium route [39,40], which is discussed further in reaction R.3.

Aside from $\overline{\mathrm{H}}$, the ionic antimatter complexes $\overline{\mathrm{H}}^+$ ($e^+\overline{p}e^+$, the antihydrogen positive ion) and $\overline{\mathrm{H}}_2^-$ ($\overline{p}e^+\overline{p}$, the antihydrogen molecular anion) are also of interest. There has been some recent discussion of possibilities for formation of these species (see, e.g., Refs. [41–44] for $\overline{\mathrm{H}}^+$ and Refs. [45–48] for $\overline{\mathrm{H}}_2^-$), and this is one of the main topics of the present work as described in particular in Sec. IV. The antihydrogen molecular anion is of particular interest since spectroscopy of transitions involving rovibrational degrees of freedom may offer enhanced sensitivity to hypothetical Lorentz and CPT violating couplings (see Ref. [49] and references therein).

The remainder of the article is organized as follows. The next section contains a summary of some of the recent experimental advances and evolving capabilities, which together suggest that it is timely to examine the basics of antimatter chemistry involving antihydrogen, while Sec. III draws on the substantial literature concerning the hydrogen chemistry relating to the early Universe. Pertinent species and reactions are identified and discussed in Sec. IV where we point out what is known and of relevance to antimatter chemistry, before summarizing in Sec. V.

II. THE POSSIBILITY OF ANTIHYDROGEN CHEMISTRY

The progress described in Sec. I has been achieved against a backdrop of technical advances with antimatter creation and storage. Positron and antiproton clouds can be formed reproducibly in the sub-20 K range [50] and routinely mixed to form $\overline{\mathrm{H}}$ [8], a fraction of which has a kinetic energy low enough to be held in ALPHA's magnetic minimum trap.

Trapping experiments typically employed by the ALPHA collaboration involved, in a single 4-min cycle, mixing around 10^5 $\overline{p}$s with about 3×10^6 e^+s at a temperature in the range 15–20 K, and resulted in the production of around 50 000 $\overline{\mathrm{H}}$s. The ALPHA magnetic minimum trap has a depth of about 0.5 K for species such as ground state $\overline{\mathrm{H}}$ with a magnetic moment of μ_B, the Bohr magneton. Around 15 or so of the nascent antiatoms were trapped per cycle, having been formed with a kinetic energy below the trap depth and with a magnetic moment aligned antiparallel to the local magnetic field (which ensures that they are the low-field seeking Zeeman species [4]). Thus, only a few 10^{-4} of the created antiatoms were held in the trap, originating from that fraction of a roughly 20 K Maxwell-Boltzmann distribution whose kinetic energies fall below the 0.5 K trap depth and which have a magnetic moment that allows capture. Simulations have shown that the $\overline{\mathrm{H}}$ is most likely to be produced in high-field seeking states [23,51] (though the trappable fraction can be improved due to the influence of e^+ collisions if n_e can be increased [27]) and that a substantial fraction of the trapped antiatoms radiatively cascade to the ground state [52].

Through optimization of the magnetic minimum trap, which has a volume of around 400 cm^3, a ground state $\overline{\mathrm{H}}$ lifetime in excess of 60 h has been obtained. Such a long lifetime has facilitated the routine accumulation, in so-called stacks which involve repeated formation and trapping cycles [8], of about 10^3 antiatoms over a period of many hours. Thus, the trapped antihydrogen density, $n_{\overline{\mathrm{H}}}^{\mathrm{trap}}$, is typically around 2 cm^{-3}.

This long $\overline{\mathrm{H}}$ lifetime, and the ability to continue to form and trap $\overline{\mathrm{H}}$ to augment the accumulated yield, has prompted our exploration of the possibility of antimatter chemistry. Such speculation is also motivated by ongoing physics advances and technical upgrades which promise to increase the trapped $\overline{\mathrm{H}}$ density, as we now explain. We note that the trapped $\overline{\mathrm{H}}$s form a positron spin-polarized sample but which can be doubly (positron and antiproton) spin-polarized by driving an appropriate ground-state hyperfine transition to a high field seeking state to leave a hyperfine pure sample, as was achieved in recent laser cooling experiments [17].

To promote $\overline{\mathrm{H}}$ chemical reactions, it is clearly beneficial to increase $n_{\overline{\mathrm{H}}}^{\mathrm{trap}}$, and there are several possibilities for this. Recent advances [53,54], using sympathetic cooling of e^+ via interaction with laser-cooled beryllium ions [55,56], has reduced T_e to 6–7 K, leading to a commensurate increase in the trappable yield to approximately 50 $\overline{\mathrm{H}}$s each mixing cycle. With further optimization, and if n_e can also be increased [27] above its current value of around 6×10^7 cm^{-3}, the number of trapped $\overline{\mathrm{H}}$s (and hence $n_{\overline{\mathrm{H}}}^{\mathrm{trap}}$) may be increased by an order of magnitude or more.

An increase in the $\overline{p}$ flux used for $\overline{\mathrm{H}}$ formation would also be beneficial. All low energy $\overline{\mathrm{H}}$ experimentation takes place at the Antiproton Decelerator (AD) facility, part of CERN's "Antimatter Factory" [57,58]. The AD typically provides 100-ns-wide pulses of around 3×10^7 $\overline{p}$s at a kinetic energy of 5.3 MeV every 100 s or so. Until recently, experiments have typically used foils to degrade the energy of the incoming beam, and although this is a simple and robust method to slow the $\overline{p}$s [59,60], only around 1 per mille of the antiparticles—those with kinetic energies below around 5–10 keV—can be dynamically captured into Penning trap-type arrangements. The latter are formed using a uniform (solenoidal) magnetic field in the tesla region, which provides confinement of charged particles transverse to its orientation, and a series of (cylindrical) electrodes arranged along the axis of the solenoid, that are biassed in a manner to provide axial confinement for the $\overline{p}$s. The latter can then be cooled and manipulated, typically using overlapping clouds/plasmas of electrons and employing a number of sophisticated techniques, similarly to those also applied to e^+ plasmas; see, e.g., Refs. [61,62] for recent

authoritative summaries. Typical antiproton densities used by ALPHA are around 10^7 cm^{-3}, though if necessary this can be increased by stacking, though further experimentation may be needed to ensure that cloud temperatures can be controlled as the density is increased.

The capabilities of the AD, and the vast array of techniques used to manipulate trapped $\overline{p}$s, have recently been augmented with the arrival of the Extra Low ENergy Antiproton (ELENA) storage ring [63,64]. ELENA takes the AD output and decelerates it to 100 keV before pulsed ejection to experiments. The ejection involves transport using electrostatic beam lines (rather than the magnetic devices used for the 5.3-MeV beam), which allows rapid and simple switching of the 100 keV $\overline{p}$s between the various experiments, facilitating operation of an antiprotons-on-demand mode of delivery and a much more efficient use of the beam. It is worth noting that this flexibility reduces the incoming number of antiparticles delivered to the experiments, with around 4.5×10^6 $\overline{p}$s available in 300 ns [64] clouds per ejection. To take advantage of this new operational mode, the ALPHA experiment operates a stand-alone $\overline{p}$ catching trap which interfaces with ELENA independently of its operation for $\overline{\mathrm{H}}$ physics. The lower energy beam allows thinner foils to be used to degrade the $\overline{p}$ kinetic energy on entry to the trapping region and has resulted in capture efficiency increases by around two orders of magnitude to ∼7% [18]. Thus, the number of $\overline{p}$s available by the ALPHA experiment has increased by over an order of magnitude, and work is ongoing to transfer this enhancement into the yield of trapped $\overline{\mathrm{H}}$. Another method, employed by the GBAR collaboration, is to use an electrostatic decelerator, which in principle is capable of decelerating particles from 100 keV to ∼1 keV without losses [65].

As mentioned briefly in Sec. I, ALPHA has recently achieved laser cooling of trapped $\overline{\mathrm{H}}$ [17]. In short, following a period of stacking in the trap [8] which resulted in the accumulation of 500–1000 $\overline{\mathrm{H}}$s over a 2- to 4-h period, the antiatoms were subject to laser irradiation at 121.6 nm to drive the $1S$-$2P$ (the Lyman-α laser cooling) transition. After a few hours of exposure of the trapped atoms to the light, their kinetic energy was found to be reduced in three dimensions [66] by around an order of magnitude to about 20 mK. Such cold atoms are then confined by a field difference of ∼60 mT, rather than 800 mT for the full trap, and as such are restricted to a volume (using the current ALPHA magnetic trap configuration) of about 80 cm^3. This corresponds to a factor of 5 enhancement in $n_{\overline{\mathrm{H}}}^{\mathrm{trap}}$, assuming all of the trapped antiatoms can be cooled. Further advances in $\overline{\mathrm{H}}$ cooling are anticipated [17] with, for instance, an improved Lyman-α laser system and optimization of the procedure. Thus, here we will assume the aforementioned factor of 5 to be a conservative gain in $n_{\overline{\mathrm{H}}}^{\mathrm{trap}}$.

We foresee that, in the near future, values of $n_{\overline{\mathrm{H}}}^{\mathrm{trap}} \gtrapprox 10^3$ cm^{-3} will be available for experimentation, with temperatures in the region of 20 mK and below. Further into the future it should be possible to confine colder clouds of $\overline{\mathrm{H}}$ into smaller volumes to promote mutual interactions of the type described below, and it may even prove possible to move cold antiatom samples into other types of atom traps in which complications due to the presence of (relatively) strong magnetic fields can be reduced or possibly eliminated.

Furthermore, the trapped $\overline{\mathrm{H}}$ samples allow the possibility of manipulating quantum states using laser and microwave transitions, as has already been exploited by ALPHA (though with the proviso that processes involving antiatom loss from the trap will have to be mitigated) and as introduced in Sec. I. This may provide ways to increase reaction rates at fixed $n_{\overline{\mathrm{H}}}^{\mathrm{trap}}$ and antiatom speed by enhancing relevant scattering cross sections. Thus, as well as an accurate knowledge of the $\overline{\mathrm{H}}$ speed distribution and the dynamical behavior of the trapped antiatoms, assessing the feasibility of observing chemical reactions involving trapped $\overline{\mathrm{H}}$ requires reliable scattering cross sections. As will be described in the remainder of this paper, much is already known from studies of reactions involving hydrogen counterparts, and we now proceed to this discussion.

III. PARALLELS WITH H CHEMISTRY IN THE EARLY UNIVERSE

Our analysis of the possibilities for $\overline{\mathrm{H}}$ chemistry have been guided, as noted by Zammit *et al.* [47], by some of the striking parallels between the ground-state antiatoms trapped with a long lifetime (alongside positrons and antiprotons) in the extreme high vacuum of ALPHA's combined magnetic minimum atom and charged particle traps, and the conditions pertaining in the early Universe when stable hydrogen atoms were formed and began to undergo chemical reactions. While the particle temperatures in current antimatter traps are much colder than the temperature of the early Universe (4000 K), the envisioned possibility of trapping larger species and controlling the population of excited states allows us to consider the complex chemistry of the early Universe.

Figure 1 presents a so-called bubble diagram illustrating the main reactions envisioned in antihydrogen chemistry. We have drawn inspiration for this from an early Universe hydrogen reaction diagram given in the review of Lepp, Stancil, and Dalgarno [67]. That work, and that of Galli and Palla [68], provide comprehensive summaries of the chemical behavior of hydrogen in the early Universe, defined to be the period when the cosmos was cold enough for atoms to survive ionization by the background radiation, namely at a temperature of around 4000 K. At this point the hydrogen density was around 10^3 cm^{-3} [67], marking the beginning of the recombination epoch, when the evolution of the Universe was controlled by atomic and molecular processes. It is noteworthy that this is the envisaged near-future value for $n_{\overline{\mathrm{H}}}^{\mathrm{trap}}$, as discussed in Sec. II.

Figure 1 illustrates interactions of positrons and antiprotons, the antimatter building blocks, mostly leading to $\overline{\mathrm{H}}$ in the first instance, and then further reactions, arranged into a number of groups (see Sec. IV), to form the more complex charged species $\overline{\mathrm{H}}^+$, $\overline{\mathrm{H}}_2^-$, and $\overline{\mathrm{H}}_3^-$ and the antimolecule $\overline{\mathrm{H}}_2$. The electron, e^-, is included in the antimatter network for two reasons: The first is due to its ability to form positronium (Ps, the e^+-e^- bound state), which can undergo positron transfer reactions, and the second is because it may assist in some reactions. Photons are also present in the network, in particular via radiative processes, and it should be noted that they can be used to stimulate reactions and produce excited states, and of course the frequencies and intensities can be tuned over a large range using laser and microwave sources to take advantage of atomic and molecular state selectivity.

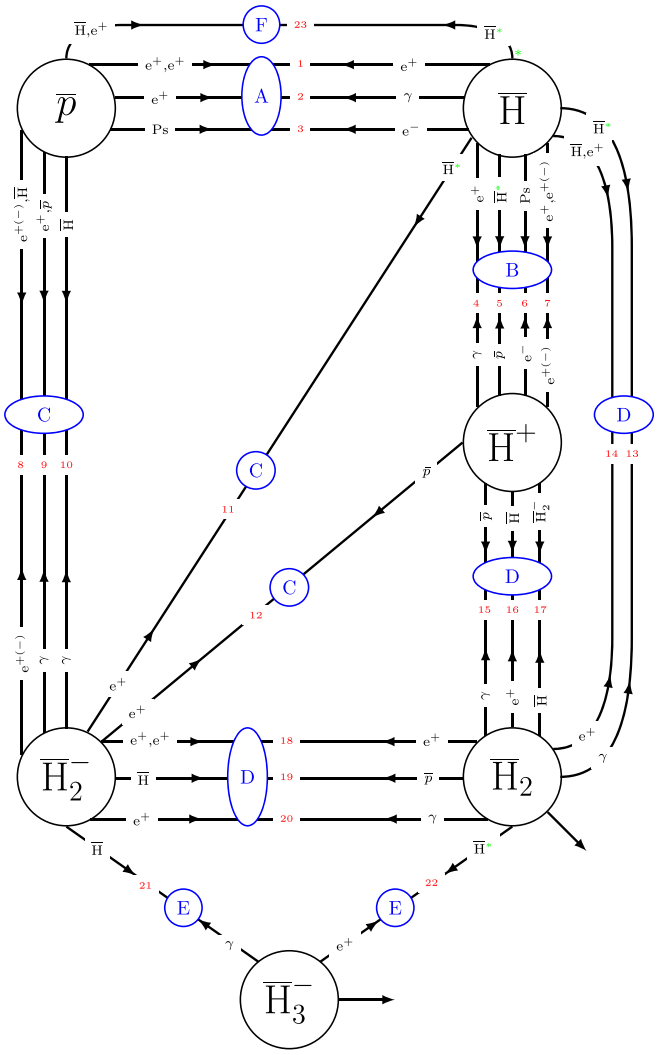

FIG. 1. Bubble diagram showing some of the important antiparticle and antihydrogen reactions, where the reaction group and number are indicated by, e.g., Ⓐ and 1, respectively; see text for details. Note that excited species may participate in, or be formed by, many of the processes and this is discussed, as appropriate, in Sec. IV. Here we denote by a star (e.g., $\overline{H}^*$) those instances when excitation is required for the process to be energetically feasible. A star has been added to the exit of the antihydrogen bubble for reaction R.23 to indicate that both of the cold $\overline{H}$ atoms need to be in excited states for this Penning ionization process to occur.

Photon stimulated (sometimes referred to as laser-stimulated) processes can be considered with chosen photon energies and intensities—and as such are likely to have a greater influence than they did in hydrogen systems in the early Universe [69]. Furthermore, experiments can be repeated with fresh batches of antiparticles, etc. (for instance to accumulate $\overline{H}$, as demonstrated by ALPHA [8] and discussed briefly in Sec. II), with controllable and reproducible [50] positron plasma parameters, n_e and T_e. Thus, in a manner not possible in the early Universe, three-body reactions such as reaction R.1, the main method (to date) of forming antihydrogen at low temperatures, can play an important role.

A further consideration for antihydrogen chemistry is loss from the trap, for which there can be annihilation with the background gas, or elastic scattering transferring enough kinetic energy for the $\overline{H}$ to escape from the trap. In addition, if excited states are present, deexcitation may result in an untrapped state and ejection from the trap. This is due to a spin-flip of the state, which may be caused by states mixing via the electric and magnetic fields present in the trap. For example, excited state $\overline{H}$-$\overline{H}$ interactions can result in spin-flip deexcitation (e.g., the reaction $\overline{H}(2S)+\overline{H}(2S)\rightarrow\overline{H}(2P)+\overline{H}(2P)$ [47]) and may need to be taken into account, depending on experimental circumstances.

We now proceed to a more detailed discussion of the reactions in the antihydrogen bubble diagram (Fig. 1), predominantly from a theoretical perspective. Our principal aim is to summarize what is known of these processes (or can be gleaned from studies of their matter counterparts) of relevance for the conditions of current and near future antihydrogen experiments and thereby point towards opportunities for further study.

IV. SPECIES AND REACTIONS

The mutual interactions of trapped $\overline{H}$ atoms, together with those involving $\overline{H}$-e^+ and $\overline{H}$-$\overline{p}$ collisions, form the basis of the antihydrogen chemistry network displayed in Fig. 1. Key species are clearly the cationic and anionic entities $\overline{H}^+$ and $\overline{H}_2^-$, not only since they form a possible gateway to heavier antimatter (see, e.g., Refs. [70,71]) but also as interesting systems in their own right (e.g., Refs. [45,46,48]). Table I contains a summary of the reactions displayed and a suggested rating to guide future work, and we now proceed to discuss each including, as appropriate, instances involving excited states or photon-assisted interactions. Note that we have appended a selection of further, typically higher-order and more complex reactions, without discussion in the main text. (See Table II in the Appendix.)

A. Group A: $\overline{H}$ formation

Within this group, the reactions most likely responsible for formation of $\overline{H}$ atoms are discussed, whether held in a neutral trap or used in a beamlike scenario.

1. Reaction R.1: $e^+ + e^+ + \overline{p} \leftrightarrow e^+ + \overline{H}$

As described in Sec. I, three-body recombination (3BR) is the main mechanism responsible for creating $\overline{H}$ atoms in, e.g., the ALPHA experiment. The energy scale of the states initially formed is $k_B T_e$; i.e., set by the temperature of the positrons. The corresponding length scale is $b = e^2/4\pi\epsilon_0 k_B T_e$ (usually termed the Thomson radius), and the velocity scale $v_e = \sqrt{k_B T_e/m_e}$, where m_e is the e^+ mass, n_e the e^+ density, and other constants have their usual meanings. It was concluded in Ref. [72] that reaction (R.1) has a rate proportional to the product of the $\overline{p}$-e^+ collision rate ($\propto n_e b^3 v_e$) and the probability that a second e^+ is close enough to carry off the binding energy ($\propto n_e b^3$), that is,

$$\lambda_{3\mathrm{BR}} = C n_e^2 v_e b^5 = C\,50.7\left(\frac{T_e}{1\,\mathrm{K}}\right)^{-4.5}\left(\frac{n_e}{10^8\,\mathrm{cm}^{-3}}\right)^2 \overline{p}^{-1}\,\mu\mathrm{s}^{-1}, \quad (1)$$

where C is a dimensionless constant.

TABLE I. Main antihydrogen chemistry reactions (as depicted in Fig. 1) with a suggested rating where 1 is of highest interest but with significant information already available, 2 of interest and would benefit from additional work, and 3 is not likely to be relevant (due to low rates of formation with current/anticipated experimental conditions).

	Reactions	Rating
	Group A: $\overline{\mathrm{H}}$ formation	
(R.1)	$e^+ + e^+ + \overline{p} \leftrightarrow e^+ + \overline{\mathrm{H}}$	1
(R.2)	$e^+ + \overline{p} \leftrightarrow \gamma + \overline{\mathrm{H}}$	2
(R.3)	$\overline{p} + \mathrm{Ps} \leftrightarrow e^- + \overline{\mathrm{H}}$	1
	Group B: $\overline{\mathrm{H}}^+$ formation	
(R.4)	$e^+ + \overline{\mathrm{H}} \leftrightarrow \gamma + \overline{\mathrm{H}}^+$	2
(R.5)	$\overline{\mathrm{H}}^* + \overline{\mathrm{H}} \leftrightarrow \overline{p} + \overline{\mathrm{H}}^+$	2
(R.6)	$\mathrm{Ps} + \overline{\mathrm{H}} \leftrightarrow e^- + \overline{\mathrm{H}}^+$	2
(R.7)	$e^+ + e^{+(-)} + \overline{\mathrm{H}} \leftrightarrow e^{+(-)} + \overline{\mathrm{H}}^+$	2
	Group C: $\overline{\mathrm{H}}_2^-$ formation	
(R.8)	$e^{+(-)} + \overline{p} + \overline{\mathrm{H}} \leftrightarrow e^{+(-)} + \overline{\mathrm{H}}_2^-$	3
(R.9)	$e^+ + \overline{p} + \overline{p} \leftrightarrow \gamma + \overline{\mathrm{H}}_2^-$	3
(R.10)	$\overline{p} + \overline{\mathrm{H}} \leftrightarrow \gamma + \overline{\mathrm{H}}_2^-$	2
(R.11)	$\overline{\mathrm{H}}^* + \overline{\mathrm{H}} \leftrightarrow e^+ + \overline{\mathrm{H}}_2^-$	2
(R.12)	$\overline{p} + \overline{\mathrm{H}}^+ \leftrightarrow e^+ + \overline{\mathrm{H}}_2^-$	2
	Group D: $\overline{\mathrm{H}}_2$ formation	
(R.13)	$\overline{\mathrm{H}}^* + \overline{\mathrm{H}} \leftrightarrow \gamma + \overline{\mathrm{H}}_2$	2
(R.14)	$e^+ + \overline{\mathrm{H}} + \overline{\mathrm{H}} \leftrightarrow e^+ + \overline{\mathrm{H}}_2$	3
(R.15)	$\overline{p} + \overline{\mathrm{H}}^+ \leftrightarrow \gamma + \overline{\mathrm{H}}_2$	3
(R.16)	$\overline{\mathrm{H}} + \overline{\mathrm{H}}^+ \leftrightarrow e^+ + \overline{\mathrm{H}}_2$	3
(R.17)	$\overline{\mathrm{H}}^+ + \overline{\mathrm{H}}_2^- \leftrightarrow \overline{\mathrm{H}} + \overline{\mathrm{H}}_2$	3
(R.18)	$e^+ + e^+ + \overline{\mathrm{H}}_2^- \leftrightarrow e^+ + \overline{\mathrm{H}}_2$	3
(R.19)	$\overline{\mathrm{H}} + \overline{\mathrm{H}}_2^- \leftrightarrow \overline{p} + \overline{\mathrm{H}}_2$	3
(R.20)	$e^+ + \overline{\mathrm{H}}_2^- \leftrightarrow \gamma + \overline{\mathrm{H}}_2$	3
	Group E: $\overline{\mathrm{H}}_3^-$ formation	
(R.21)	$\overline{\mathrm{H}} + \overline{\mathrm{H}}_2^- \leftrightarrow \gamma + \overline{\mathrm{H}}_3^-$	3
(R.22)	$\overline{\mathrm{H}}^* + \overline{\mathrm{H}}_2 \leftrightarrow e^+ + \overline{\mathrm{H}}_3^-$	3
	Group F: $\overline{\mathrm{H}}$ destruction	
(R.23)	$\overline{\mathrm{H}}^* + \overline{\mathrm{H}}^* \leftrightarrow e^+ + \overline{p} + \overline{\mathrm{H}}$	1

Three-body recombination almost always results in a very loosely bound antihydrogen, which is not stable against re-ionization in further collisions with positrons. To stabilise the antiatom it has to increase its binding energy, which also can be the result of further collisions. The time evolution of the state of the antiatom can be seen as a random walk in binding energy, where most trajectories end up in re-ionization of the antiatom, but a few eventually lead to deeply bound antihydrogen atoms.

Therefore, the overall rate of three-body recombination cannot be calculated from a single cross section, but is the result of an initial three-body collision followed by a number of two-body collisions, and moreover this usually has to be repeated several times before an attempt is successful. Thus the three-body recombination rate has to be defined as the rate at which antiatoms flow from zero binding energy to states with binding energies much larger than $k_B T_e$. This process has been investigated by several authors who have found that this rate goes through a minimum or "bottleneck" at a few times $k_B T_e$ [21,23,72,73]. The constant C in Eq. (1) is determined from the flow through this bottleneck. It can be obtained from Monte Carlo simulations, where many individual antihydrogen trajectories are followed in time, from an initial loosely bound state to either ionization or formation of a stable antihydrogen with binding energy exceeding the bottleneck energy. After some time the distribution of binding energies reaches a steady state, with a constant flow of antiatoms crossing the bottleneck. Simulations of this steady-state flow rate give $C = 0.76$ [74] (for the field-free case).

In experiments that use only a Penning-Malmberg trap to confine the charged particles (see Sec. II) the recombination takes place in a near uniform magnetic field B along the axis of the trap. In the case of ALPHA a magnetic minimum antihydrogen trap is superimposed on the charged particle trap, and as such there is a small (below 0.1% of the on-axis field) nonuniformity close to the center of the trap where the antiatoms are formed. The magnetic field can be quantified by the magnetization parameter $\chi = v_e/\Omega_c b$, where $\Omega_c = eB/m_e$ is the cyclotron frequency of the positrons. In the ALPHA experiment $B = 1$ T and $T_e \simeq 10$ K, giving $\chi \simeq 0.04$. Simulations show that the magnetization has a drastic effect on the three-body recombination rate. In the limit $B \to \infty$ ($\chi = 0$) it is reduced by an order of magnitude to $C = 0.070$ [72]. At experimentally relevant magnetizations, $C \simeq 0.11$ was obtained for χ in the range 0.002–0.03 by Robicheaux and Hanson [21], while Bass and Dubin [23] obtained $C = 0.10$ at $\chi = 0.001$ and $C = 0.14$ at $\chi = 0.005$.

As discussed above, these rates assume that a steady-state distribution of binding energies has had time to establish. Robicheaux [75] recognized that this does not correspond to the situation in many experiments. Instead, the antiprotons pass back and forth through the positron plasma, spending only a finite time inside during each pass. Between passes the formation process is stopped and restarted at the next pass through the plasma. Thus the steady-state picture is not appropriate. In recent experiments, formation has been enhanced through a meticulous optimization of the way antiprotons and positrons are mixed which reduces this effect [8].

Another assumption in many simulations is that the antiproton/antihydrogen is infinitely massive and thus does not move. Due to its larger mass the speed of the antiproton along the axis of the trap will indeed be much slower than that of the positrons. However, in the plane perpendicular to the axis the antiprotons and positrons perform a $\mathbf{E} \times \mathbf{B}$ drift motion around the trap axis. The electric field here arises from the space charge of the positron plasma and will thus increase with radial distance from the trap axis. Simulations have shown that this motion has important effects for the rate of recombination [25], in particular when coupled to the cycles of three-body formation and subsequent ionization [26].

The above-mentioned complications arising in experimental situations make it difficult to define a definite formation rate. On the other hand, because antiprotons are delivered to experiments in bunches separated by 1–2 min, the actual *rate* of formation is only important when compared to other experimental rates, e.g., the rate of heating of the positron plasma or the rate of radial expansion of both positrons and antiprotons. Of more direct experimental relevance is the *fraction* of injected antiprotons which eventually results in stable antihydrogen. This fraction is the result of a complex interplay between the different effects discussed above. Further conditions can also be imposed, such as the requirement that the resulting antihydrogen is in a state that can be magnetically trapped (i.e., in a low-field seeking state and with kinetic energy less that the trap depth) [27,76,77] or has beamlike properties (i.e., collimated movement in sufficient numbers) [28].

To gain insight into competing formation processes, here we utilize an idealized case scenario. A three-body recombination rate can be determined utilizing the principle of detailed balance (or microscopic reversibility, MR) from the collisional ionization rates (or cross sections). With this approach, the positron three-body recombination rate coefficient (units of $\mathrm{cm}^6\,\mathrm{s}^{-1}$), $\alpha^{\mathrm{3BR}}_{u\to l}(T_e)$, can be related to the e^+-$\overline{\mathrm{H}}$ impact ionization (PII) rate coefficient, $\alpha^{\mathrm{PII}}_{l\to u}(T_e)$, such that [78]

$$\alpha^{\mathrm{3BR}}_{u\to l}(T_e) = 1.657\times10^{-22}\,\frac{g_l}{g_u}\,\frac{e^{E_l/k_BT_e}}{(k_BT_e/\mathrm{eV})^{3/2}}\,\alpha^{\mathrm{PII}}_{l\to u}(T_e), \quad (2)$$

for a Maxwellian distribution of free-positrons at a temperature T_e. Here g_l and g_u are the statistical weights (or degeneracy factors) of the "lower" l state and "upper" u state, respectively, and E_l is the ionization energy of the l state. Here we utilize the (field-free isolated atom) classical Gryzinski electron-impact ionization approach [79] to calculate cross sections and perform the standard rate coefficient calculation,

$$\alpha^{\mathrm{PII}}_{l\to u}(T_e) = \int \sigma^{\mathrm{PII}}_{l\to u}(E)v_e(E)f(E,T_e)dE, \quad (3)$$

where we take $f(E,T_e)$ as a Maxwellian energy distribution function and v_e is the relative speed of the positron (with respect to $\overline{\mathrm{H}}$ assumed here to be at rest) as a function of energy [according to $f(E,T_e)$]. For now, in order to avoid solving the full collisional-radiative rate matrix or tracking particles via a Monte Carlo simulation, here we sum the total three-body recombination rate per antiproton,

$$\lambda^{\mathrm{3BR}}(T_e) = \sum_l n_e^2\alpha^{\mathrm{3BR}}_{u\to l}(T_e), \quad (4)$$

where the summation over bound l states is truncated to include only lower states that have a binding energy above the bottleneck binding energy condition, taken here as $4k_BT_e$. Contrary to Eq. (1), this approach does not include multistep processes, such as three-body recombination (to an l state below the bottleneck binding energy) followed by collisional deexcitation processes that would result in population above the bottleneck binding energy. Results from these two approaches are presented in Fig. 2 at several values of T_e in the range 5–500 K and for n_e between 5×10^6 and $2\times10^8\ \mathrm{cm}^{-3}$. From these comparisons it is clear that simulations predict recombination rates about two orders of magnitude larger than the MR 3BR estimate. This result shows, and as discussed above, the major contribution to recombination come from collisional deexcitation processes, which dominate in the formation of antihydrogen states bound deeply enough for detection and trapping.

2. *Reaction R.2:* $e^+ + \overline{p} \leftrightarrow \gamma + \overline{\mathrm{H}}$

Spontaneous radiative recombination (SRR, reaction R.2) has been noted as a possible source of $\overline{\mathrm{H}}$ for some time, initially in the context of merged positron and antiproton beams in storage rings [80]; see also the discussions in Müller and Wolf [81], Holzscheiter *et al.* [82], and Meshkov and Skrinsky [83]. The cross section for this process has long been known (e.g., Ref. [84]) and can be given numerically for capture into an antihydrogen state with principal quantum number $n_{\overline{\mathrm{H}}}$ as

$$\sigma^{\mathrm{SRR}}(n_{\overline{\mathrm{H}}},T_e) = \frac{2\times10^{-22}\mathrm{Ry}}{n_{\overline{\mathrm{H}}}k_BT_e\left(1+n^2_{\overline{\mathrm{H}}}k_BT_e/\mathrm{Ry}\right)}\,\mathrm{cm}^2, \quad (5)$$

where Ry is the Rydberg of energy, and T_e has been defined previously and here represents the effective temperature of the positron in the continuum. Given that in typical $\overline{\mathrm{H}}$ experiments, $\mathrm{Ry} \gg k_BT_e$, for the states of most interest (i.e., those at low $n_{\overline{\mathrm{H}}}$) Eq. (5) can be adequately approximated by

$$\sigma^{\mathrm{SRR}}(n_{\overline{\mathrm{H}}},T_e) \approx \frac{2\times10^{-22}\mathrm{Ry}}{n_{\overline{\mathrm{H}}}k_BT_e} = \frac{3.2\times10^{-17}}{n_{\overline{\mathrm{H}}}\,(T_e/\mathrm{K})}\,\mathrm{cm}^2, \quad (6)$$

with a related expression in terms of the positron speed, v_e, as $\sigma^{\mathrm{SRR}}(n_{\overline{\mathrm{H}}},v_e) \approx 9.6\times10^{-10}/n_{\overline{\mathrm{H}}}v_e^2$ (cm^2 and with v_e in ms^{-1}).

The latter cross section can be used to compute a rate coefficient, α^{SRR}, using the standard convention, e.g., Eq. (3). This allows the overall rate, λ^{SRR}, of $\overline{\mathrm{H}}$ production per antiproton to be estimated from the positron density and this is simply given by

$$\lambda^{\mathrm{SRR}} = \sum_{n_{\overline{\mathrm{H}}}} \alpha^{\mathrm{SRR}}(n_{\overline{\mathrm{H}}})n_e. \quad (7)$$

Note that λ^{SRR} is the total spontaneous capture rate to all bound states and integrated over the entire positron energy spectrum in the continuum. The SRR rates have also been calculated via the MR approach, using Kramer's semiclassical photoionization cross sections and the sum over recombination states is truncated to include only states with binding energy above the bottleneck binding energy (again taken here as $4k_BT_e$). These results are presented in Fig. 2, showing that the MR results are in excellent accord with those from the analytic approach described above. Except at the highest T_e

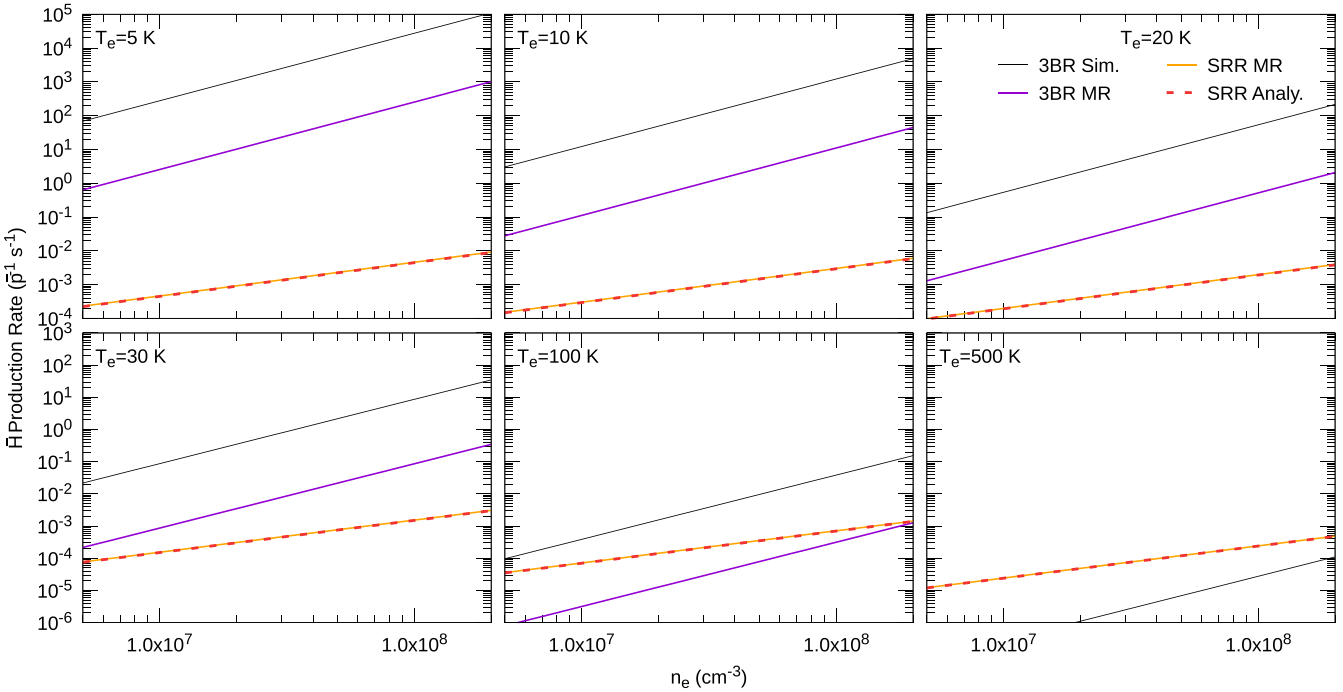

FIG. 2. The $\overline{\mathrm{H}}$ production rate from three-body recombination (3BR) and spontaneous recombination (SRR); assuming $B = 0$ and summing the recombination rates into states above the bottleneck binding energy. The 3BR results were calculated via Eq. (1) with $C = 0.76$ [74] (includes collisional dexcitation) and via MR of the e^+-$\overline{\mathrm{H}}$ impact ionization cross sections. The SRR results were calculated via Eq. (6) and via MR of the photoionization cross sections (see the text for details).

($\gtrsim$100 K), the 3BR $\overline{\mathrm{H}}$ formation rates greatly exceed those for SRR for most of the range of n_e investigated. The rates become comparable at $n_e = 5 \times 10^6$ cm^{-3} and 100 K, and by 500 K the SRR rate exceeds that for 3BR at all densities up to the maximum shown. In this instance, overall $\overline{\mathrm{H}}$ production rates are low (below 10^{-3} $\overline{p}^{-1}$ s^{-1}): Thus, high T_e effectively damps antiatom production, as exploited in early experiments by ATHENA [2,85].

Photon stimulated radiative recombination [PSRR, namely $e^+ + \overline{p} + N_\gamma\gamma \leftrightarrow (N_\gamma + 1)\gamma + \overline{\mathrm{H}}$, where here N_γ is the number of photons], which was observed some time ago for the electron-proton (e^--p) system [86,87], will typically apply laser radiation to stimulate capture from the continuum to a particular atomic state. There are, however, a number of variations on this process including: two-color stimulation, for instance involving capture into an upper quantum state, followed by stimulation to a lower state (see, e.g., Refs. [81,88,89]) and so-called laser-assisted radiative recombination [90], which is a nonresonant version of PSRR with a different frequency photon emitted in the final state. Aspects of PSRR have been reviewed in the context of $\overline{\mathrm{H}}$ experimentation elsewhere [82,91] and the ATHENA collaboration unsuccessfully attempted to promote formation of the $\overline{\mathrm{H}}$ $n_{\overline{\mathrm{H}}} = 11$ state via irradiation at just over 0.1 eV using an intense CO_2 laser [92].

It should be noted that most of the early discussions of PSRR were formulated for in-beam and storage ring scenarios rather than the environment typical of $\overline{\mathrm{H}}$ and antiparticle traps that was described briefly in Sec. II. For the present purposes we assign a single temperature T_e to the e^+ cloud, with which the overlapping $\overline{p}$s are in equilibrium. Given the mass difference of the two species, the latter can, for the present purposes, be considered at rest in the positrons.

Considering PSRR to involve capture of a e^+ from a narrow continuum (a few $k_B T_e$ wide) using laser radiation with a frequency bandwidth, Δf, and ignoring the bandwidth of the atomic state the gain, G, due to the PSRR processes is defined by [91]

$$\lambda^{\mathrm{PSRR}}(n_{\overline{\mathrm{H}}}, \Delta f) = G\lambda^{\mathrm{SRR}}, \tag{8}$$

with $\lambda^{\mathrm{PSRR}}(n_{\overline{\mathrm{H}}}, \Delta f)$ the stimulated capture rate to a state with quantum number $n_{\overline{\mathrm{H}}}$ relevant to the laser. General features concerning the evaluation of G have been discussed elsewhere [91], and will clearly be specific to the experimental arrangement. Note that the storage ring [86] and merged beam single pass [87] experiments found G in the range 10–100. It is of particular pertinence to recall that Eq. (8) does not explicitly include duty cycle effects, for instance if pulsed lasers are used for intensity and bandwidth considerations, which may limit the utility of the technique. Further theoretical work on this topic would be welcome, particularly if low-lying excited $\overline{\mathrm{H}}$ states (such as the $2S$ state) can be selectively populated.

3. *Reaction R.3:* $\overline{p} + \mathrm{Ps} \leftrightarrow e^- + \overline{\mathrm{H}}$

The $\overline{p}$-Ps process (reaction R.3) has long been posited as a source of cold $\overline{\mathrm{H}}$ [93–95]. A p-Ps test experiment was performed some time ago [96] and the reaction has recently been observed by the AEgIS [39] and GBAR [40] collaborations. In the AEgIS experiment, which took place in a 1-T magnetic field, the reaction was promoted by laser excitation to a selection of Rydberg Ps levels around the (field-free) $n_{\mathrm{Ps}} = 17$ manifold, with n_{Ps} as the Ps principal quantum number. Part

of the continued interest in this reaction stems from the possibility of enhancing reaction rates and controlling the formed $\overline{\mathrm{H}}$ using laser-excited Ps, and that the production of Rydberg Ps is now routine. A useful review of Ps physics and related experimental capabilities has been given by Cassidy [97]. It should also be noted here that Storry and colleagues [98] have observed reaction R.3 using a Double-Rydberg resonant charge exchange method devised by Hessels *et al.* [99].

There is extensive theoretical literature on reaction R.3, which is related to the time reverse and charge conjugate process of Ps formation in e^+-H collisions. For ground-state species this is a well-studied system, and benchmark data are available [100]. For the present purposes, however, it will suffice to provide a short resumé of some of the most recent theoretical work on the reaction. This has involved use of the sophisticated convergent close coupling (CCC) quantum scattering approach [101–105] complemented and supplemented with data using a classical trajectory Monte Carlo (CTMC) methodology [106–110].

Cross-section data for reaction R.3 are typically given for scenarios in which either the $\overline{p}$s or the Ps are fixed (corresponding to experimental geometries), though can easily be manipulated to provide reaction rate coefficients, if desired, by forming the product of the Ps density, the charge transfer cross section for the particular Ps state and the relative Ps/antiproton speed. The process always has exothermic channels available (since there are available $\overline{\mathrm{H}}$ states with binding energies greater than those for Ps for any state of the latter), and as such the cross sections exhibit threshold behavior [111] resulting in characteristic dependencies at low energies. For $n_{\mathrm{Ps}} = 1$ the short-range nature of the antiproton-Ps interaction results in the cross section following standard threshold laws [112], varying as $0.18 \times 10^{-16}/\sqrt{E}\ \mathrm{cm}^2$ as $E \to 0$ (where here E is the center-of-mass energy in eV). Thus, the product $\sigma v = 7.4 \times 10^{-10}\ \mathrm{cm}^3\,\mathrm{s}^{-1}$ becomes energy-independent at low energies, and can easily be multiplied with the appropriate density to yield a rate. For excited states, on the other hand, the long-range interaction is dipole dominated, and leads to the cross section rising as $1/E$ at low energies [113]. The most recent work on this topic [110] has provided an invaluable comparison between the best available quantum model (CCC) and results from a CTMC model. This study has included results for reaction R.3 and the competing processes of Ps break-up and state change and has not only produced definitive data for the processes calculated, but also recommendations for the use of scaling laws to derive data for higher values of n_{Ps}. For $n_{\mathrm{Ps}} = 2, 3$ the cross section grows by orders of magnitude. Taking the cross section at $E = 10^{-5}$ eV, it is $5.6 \times 10^{-15}\ \mathrm{cm}^2$ for $n_{\mathrm{Ps}} = 1$ and grows to $\sim 10^{-10}\ \mathrm{cm}^2$ for $n_{\mathrm{Ps}} = 2$ and by another order of magnitude for $n_{\mathrm{Ps}} = 3$. For more highly excited states CTMC simulations predict a scaling $\propto n_{\mathrm{Ps}}^4$ [106], but, surprisingly, CCC calculations found more modest increases $\propto n_{\mathrm{Ps}}^2$. The mechanism for this suppression was elucidated in Ref. [104] and arises because the competition between the long-range dipole interaction and centrifugal potential, both with a r^{-2} dependence.

Realizing reaction R.3 experimentally is challenging. The GBAR collaboration recently reported a small number of $\overline{\mathrm{H}}$ formed using ground-state positronium [40]. With laser excitation of positronium and increased positronium densities, envisaged for the future, enough $\overline{\mathrm{H}}$ to form the $\overline{\mathrm{H}}^+$ through reaction R.6 (see below) should be possible.

B. Group B: $\overline{\mathrm{H}}^+$ formation

In this section, those reactions of possible use to form the cationic $\overline{\mathrm{H}}^+$ species are discussed.

1. Reaction R.4: $e^+ + \overline{\mathrm{H}} \leftrightarrow \gamma + \overline{\mathrm{H}}^+$

We now turn to formation of $\overline{\mathrm{H}}^+$ via reaction R.4. The matter equivalent of this direct radiative process, or more properly the time reverse reaction photodetachment of H^-, has been of interest for decades due to its importance in solar physics. There is one bound state ($1\mathrm{s}^2\ {}^1\mathrm{S}_0^e$) around 0.75 eV below the (e^-+H) continuum, and there have been several recent studies of the process undertaken with the formation of $\overline{\mathrm{H}}^+$ in mind [42–44]. The cross sections, and hence the reaction rates for the direct radiative capture are well established [42,43] down to the very low temperature range (typically in the kelvin region) that is relevant for antimatter studies (since the reaction will necessarily involve trapped $\overline{\mathrm{H}}$). Unfortunately reaction rates are low with the rate coefficient varying roughly linearly at low positron temperatures approximately as $\alpha_{\overline{\mathrm{H}}^+}^{\mathrm{SRR}}(T_e) \approx 10^{-18}(T_e/\mathrm{K})\ \mathrm{cm}^3\,\mathrm{s}^{-1}$, which is approximately seven orders of magnitude lower than the corresponding $\overline{\mathrm{H}}$ reaction R.2 (SRR) rate coefficient (which were shown in Fig. 2).

An added complication is the possibility of heating the trapped antiatoms by the dense positron cloud, though as highlighted in Sec. II recent progress has been made in using sympathetic cooling to lower T_e into the few kelvin range [54], and laser cooling of antihydrogen has also been reported recently [17]. A full simulation of trapped $\overline{\mathrm{H}}$ interacting with positrons in the presence of active laser cooling is probably worthwhile in order to provide a realistic estimate for $\overline{\mathrm{H}}^+$ yields under conditions appropriate to current and foreseen experiments.

Increasing $\overline{\mathrm{H}}^+$ yields using the stimulated version of reaction R.4 has also been considered recently [44,114]. Explicit formulas and examples are given by Jacob and coworkers [44], who also point out some of the general features of the reaction. These are, most notably, that the laser electric field (which defines its intensity) should be much less than that of the ionic core acting on the loosely bound positron, and that the laser frequency should be resonant with respect to the energy of the transition leading to the formation of the bound state. The latter defines the energy of the laser photons. It was also pointed out [44], any enhancement over the direct radiative process (essentially the equivalent of G in the discussion of reaction R.2) only applies to a positron energy range defined by laser parameters. Further work is warranted to align this theoretical effort more closely to experimental conditions.

2. Reaction R.5: $\overline{\mathrm{H}}^* + \overline{\mathrm{H}} \leftrightarrow \overline{p} + \overline{\mathrm{H}}^+$

Reactions of pairs of antihydrogen atoms, in which (at least) one of them is excited can lead to the production of $\overline{\mathrm{H}}^+$,

$\overline{\mathrm{H}}_2^-$, and $\overline{\mathrm{H}}_2$. For the $\overline{\mathrm{H}}^+$ case (i.e., the charge transfer reaction R.5), in the limit of zero collision energy, the excited $\overline{\mathrm{H}}$ must be in a state for which $n_{\overline{\mathrm{H}}} \geqslant 5$, while for $n_{\overline{\mathrm{H}}} = 4$ the reaction channel opens at a collision energy of 0.1 eV.

Reaction R.5 is also energetically allowed in collisions of two $\overline{\mathrm{H}}$ atoms both excited to the $2S$ state. Vogel [115] discusses a mechanism where an excited metastable state of the ion is created in an initial resonant collision, which, as a multistep process, is expected to be significantly suppressed at low particle densities.

Most work, experimental and theoretical, has been directed at the reverse, charge conjugate reaction of R.5, i.e., the mutual neutralization of p and H^-. In the early 1970s the cross sections for mutual neutralization were measured, and used to derive rate coefficients (see [68] for details) with sizable uncertainties at the lowest temperatures. Studies have continued with significant improvements to the experimental measurements (with results differing significantly from the early measurements) as well as to numerical calculations [116–119]. Good agreement currently exists between experiment [120,121] and theory at ∼10 eV, with calculations continuing to the millielectronvolt level, where the numerical results, in contrast to experiments, follow the Wigner law, $\sigma \simeq 2 \times 10^{-14}(E/\mathrm{eV})^{-1}\ \mathrm{cm}^2$ and a rate coefficient of $\alpha(T_{\overline{\mathrm{H}}}) \sim 3 \times 10^{-6}(T_{\overline{\mathrm{H}}}/\mathrm{K})^{-0.5}\ \mathrm{cm}^3\ \mathrm{s}^{-1}$ has been calculated [116] (where E is the antihydrogen kinetic energy and $T_{\overline{\mathrm{H}}}$ the equivalent temperature).

From these calculations of mutual neutralization, cross sections for the direct charge transfer process have also been derived [122]. At $E = 10^{-5}$ eV the cross sections in collisions between ground-state hydrogen and atoms excited to $5S$ or $6S$ lie in the vicinity of $10^{-14}\ \mathrm{cm}^2$, while for $7S$ the cross section is $\sim 6 \times 10^{-15}\ \mathrm{cm}^2$. Thus the trend observed in calculations is lower cross section for higher excited states. At lower energies Wigner's law predicts a $1/\sqrt{E}$ dependence on energy. For $4S$, the cross section at the threshold energy is $\sim 7 \times 10^{-16}\ \mathrm{cm}^2$. While the rate coefficient in the low-energy limit turns out to be $\sim 10^{-10}\ \mathrm{cm}^3\ \mathrm{s}^{-1}$ making this reaction difficult to observe, there are indications that the system has resonances at relatively low energies, that potentially could give higher reaction rates. Furthermore, it may be useful to consider this reaction when both antihydrogen atoms are in excited states, e.g., $2S$+$2S$ collisions: to the best of our knowledge data are not currently available for such cases.

3. *Reaction R.6:* $\mathbf{Ps + \overline{H} \leftrightarrow e^- + \overline{H}^+}$

The mechanism to produce $\overline{\mathrm{H}}^+$ via charge exchange in $\overline{\mathrm{H}}$-Ps collisions was suggested by Walz and Hänsch [41] as a means to produce the anti-ion as an intermediary for the eventual creation of ultracold $\overline{\mathrm{H}}$ atoms for a test of the WEP for antimatter, and will form the centrepiece of the experimental programme of the GBAR Collaboration [123]. This is the motivation for recent calculations of reaction R.6 for Ps both in its ground state or in a low-lying excited state [124–130].

The calculations in Refs. [124–127] use the Coulomb distorted wave-final state (CDW-FS) method, employing analytical approximations, with varying degrees of sophistication for the $\overline{\mathrm{H}}^+$ wave function. This is a perturbative method akin to the Coulomb-Born approximation, so its validity at low energies can be questioned.

A very different approach was taken in Refs. [128–130]. This method, known as the coupled-rearrangement channel (CRC) uses a very accurate description of the wave function at low energies but becomes very cumbersome for energies much above the formation threshold. At these energies the CDW-FS results are generally a few times larger than the CRC results, but the methods should converge at higher energies. Unfortunately, the CRC results have not yet been extended to energies where the CDW-FS method is reliable. In addition to production of $\overline{\mathrm{H}}^+$, the CRC method also gives cross sections for elastic Ps-$\overline{\mathrm{H}}$ scattering and competing inelastic processes such as (de-)excitation and (de-)polarization of Ps.

Results using the CDW-FS [127] and CRC [129] methods have been presented only for Ps principal quantum numbers $n_{\mathrm{Ps}} \leqslant 3$, where the reaction is endothermic. For collisions with ground state $\overline{\mathrm{H}}$ the threshold energy is 6.05 eV in the center-of-mass frame (corresponding to a $\overline{\mathrm{H}}$ impinging on a stationary Ps with a kinetic energy of 5.56 keV), for $n_{\mathrm{Ps}} = 2$ it is 0.95 eV and for $n_{\mathrm{Ps}} = 3$ it is only 0.0017 eV. It should be noted that the relevant regime for the GBAR experiment is $\overline{\mathrm{H}}$ energies $\gtrsim$1 keV (corresponding to a center-of-mass energy 1.1 eV).

Because of the near degeneracy between the initial and final channels, one would perhaps expect that formation from $n_{\mathrm{Ps}} = 3$ would have the largest cross section at threshold. However, according to the CRC calculations the $2P$ state has the largest formation cross section, $2.4 \times 10^{-15}\ \mathrm{cm}^2$, followed by $1.3 \times 10^{-15}\ \mathrm{cm}^2$ for $2S$ (in accordance with threshold laws these cross sections are roughly constant for energies within $\lesssim$0.1 eV of the threshold). Thus, the increase is rather modest compared to the cross section $5.5 \times 10^{-16}\ \mathrm{cm}^2$ for ground-state Ps. For $n_{\mathrm{Ps}} \leqslant 2$, $\overline{\mathrm{H}}^+$ formation is the dominating inelastic channel, while for all initial states with $n_{\mathrm{Ps}} = 3$ the CRC results show that deexcitation and (de-)polarization of positronium dominates over $\overline{\mathrm{H}}^+$ formation. The reason for this has not been fully clarified. It might also be useful to have states with $n_{\mathrm{Ps}} > 3$ investigated, since the reaction for such species is exothermic, and hence the cross section should be proportional to $1/\sqrt{E}$ at low energies.

4. *Reaction R.7:* $\mathbf{e^+ + e^{+(-)} + \overline{H} \leftrightarrow e^{+(-)} + \overline{H}^+}$

This dileptonic (di) three-body recombination process is discussed briefly by Jacob *et al.* [44] with the reaction involving only e^+s found to be of low rate due to the repulsion between the colliding like charges. Further consideration has been provided by Jacob *et al.* [131], with a more detailed examination of the electron-mediated variant. Inferring the behavior of the rate coefficient, α^{di}, for this reaction from their presented data, it would seem to have only a weak variation with T_e below about 100 K, which may bode well for future study. Their presented rate data allows the coefficient at low T_e to be extracted by dividing by their assumed values for positron and electron cloud densities to find $\alpha^{\mathrm{di}} \approx 5 \times 10^{-24}\ \mathrm{cm}^6\ \mathrm{s}^{-1}$. Comparing to the low temperature radiative combination rate of reaction R.4 [42,43] we find the ratio $\lambda^{\mathrm{di}}/\lambda^{\mathrm{rad}} \approx 5 \times 10^{-6}(n_{e^-}/\mathrm{cm}^3)/(T_e/\mathrm{K})$, with n_{e^-} the electron density. Thus, though both processes are low rate given current experimental capabilities, the dileptonic reaction may

have advantages over the direct radiative process for the production of $\overline{\mathrm{H}}^{+}$, particularly if using cold leptons.

However, it should be borne in mind for this reaction that there will be competition with the $\overline{\mathrm{H}}$ + Ps final state, and data will be needed for this process to assess experimental viability. It may be feasible to extract rates for the latter, since the time reverse, charge conjugate reaction is Ps break-up in Ps-H collisions. Furthermore, to the best of our knowledge there have been no experimental studies of combined, low temperature, e^{+}-e^{-} plasmas, which would seem to be worthwhile in the context of the present discussion.

C. Group C: $\overline{\mathrm{H}}_2^{-}$ formation

In this section candidate reactions for the formation of the key anionic species, $\overline{\mathrm{H}}_2^{-}$, are discussed. It is worth prefacing this discussion by noting that the structure of the matter equivalent $\overline{\mathrm{H}}_2^{-}$ does lean favorably to its formation through electronic excited states. These excited states are practically all repulsive or have shallow minima at relatively large internuclear separations compared to the electronic ground state [132–137]. As a result, population in these electronic excited states predominately lead to radiative decay dissociation of the molecule or radiative decay to the very highest-lying rovibrational levels of the electronic ground state. Therefore, here, we only consider formation of $\overline{\mathrm{H}}_2^{-}$ via direct channels to the electronic ground state (omitting stepwise processes).

1. Reaction R.8: $e^{+(-)} + \overline{p} + \overline{\mathrm{H}} \leftrightarrow e^{+(-)} + \overline{\mathrm{H}}_2^{-}$

Three-body association (3BA) to form $\overline{\mathrm{H}}_2^{-}$ is the reverse reaction of positron-impact dissociative-excitation. Dissociative-excitation of $\overline{\mathrm{H}}_2^{-}$ can proceed via two pathways: a resonant process, where $\overline{\mathrm{H}}_2^{**}$ is temporarily formed and is followed by autoionization of the target in the vibrational continuum, and a direct process, where $\overline{\mathrm{H}}_2^{-}$ is excited to the vibrational continuum (via electronic excitation to a repulsive potential energy curve within the Franck-Condon envelope). The resonant process has been studied extensively with the multichannel quantum defect theory [138–141], where cross sections for e^{-}+H_2^{+} have been calculated for the full range of vibrational levels of the electronic ground state [138,140]. The direct process has been calculated with the CCC approach for a subset of vibrational levels of the electronic ground state [135,136].

Using the principle of detailed balance, the positron-impact dissociative-excitation rate coefficient, $\alpha^{\mathrm{PIDE}}_{l\rightarrow u}(T)$, can be related to the reverse three-body association rate coefficient (units of $\mathrm{cm}^6\,\mathrm{s}^{-1}$), $\alpha^{\mathrm{3BA}}_{u\rightarrow l}(T)$ via

$$\alpha^{\mathrm{3BA}}_{u\rightarrow l}(T) = 4.256\times10^{-27}\frac{g_{\mathrm{W}l}}{g_{\mathrm{X}u'}g_{\mathrm{Y}u''}}e^{E_0/k_BT}\left(\frac{\mathrm{Da\,eV}}{\mu_{\mathrm{XY}}k_BT}\right)^{3/2} \times \alpha^{\mathrm{PIDE}}_{l\rightarrow u}(T), \tag{9}$$

where $g_{\mathrm{W}l}$, $g_{\mathrm{X}u'}$, and $g_{\mathrm{Y}u''}$ are the statistical weights of the lower and upper levels of the molecule, atom and ion respectively, μ_{XY} is the reduced mass of the products X and Y (in units of daltons), and E_0 is the dissociation energy for the transition. Here we have assumed Maxwellian distributions for all the particles and that they are at the same temperature. We estimate the importance of this process by utilizing the vibrationally resolved dissociative-excitation cross sections fit by Janev *et al.* [142] and calculate the total rate coefficient for association into the electronic ground state. Note here the sum is truncated at $v = 18$ (due to the availability of the Janev *et al.* [142] data), where the final vibrational bound state $v = 19$ is bound by 0.71 cm^{-1} [143] (in the Born-Oppenheimer approximation). The total rate, λ^{3BA}, of $\overline{\mathrm{H}}_2^{-}$ production per $\overline{\mathrm{H}}$ is $\lambda^{\mathrm{3BA}} = \sum_l \alpha^{\mathrm{3BA}}_{u\rightarrow l}(T) n_{\overline{p}} n_e$. From 5 to 30 K, the total three-body association rate coefficient ranges from $\alpha^{\mathrm{3BA}}(T) \approx 10^{-36}$–$10^{-33}\,\mathrm{cm}^6\,\mathrm{s}^{-1}$ and hence a total rate $\lambda^{\mathrm{3BA}} \approx 10^{-20}$–$10^{-17}\mathrm{s}^{-1}$ per $\overline{\mathrm{H}}$ when setting $n_e \sim n_{\overline{p}} \sim 10^8\ \mathrm{cm}^{-3}$. It may be feasible to increase these densities at higher positron temperatures, though it is likely that collisional heating will result in ejection of the antihydrogen from the atom trap.

For the electron assisted three-body association reaction, we estimated the rate coefficient using the equivalent e^{+}+H_2^{+} dissociative excitation cross section calculated by Mori *et al.* [144]. Since these calculations were performed for a single internuclear separation that approximated scattering from the vibrational ground state, we energetically shifted these cross sections to represent dissociative excitation from vibrationally excited states (no attempt was made in correcting for the magnitude of the cross sections). The energy shift was calculated from the vertical excitation energy at the vibrational states mean internuclear separation, where the accurate potential energy curves of Zammit *et al.* [143] were used. Using the above form of the three-body association rate coefficient (which assumes the particles are at the same temperature), we calculated a rate coefficient $\alpha^{\mathrm{3BA}}(T) \approx 5\times10^{-41}$–$5\times10^{-38}\ \mathrm{cm}^6\,\mathrm{s}^{-1}$ for temperatures 5–30 K. These are five orders of magnitude below the aforementioned positron rates, presumably due to the repulsive interaction between the electron and the antiproton. We also note that the dissociative excitation process and vibrational deexcitation processes will influence the overall production rate.

2. Reaction R.9: $e^{+} + \overline{p} + \overline{p} \leftrightarrow \gamma + \overline{\mathrm{H}}_2^{-}$

This radiative associative recombination (RAR) process is the reverse of the total break-up, or photodissociative-ionization, of $\overline{\mathrm{H}}_2^{-}$. The charge conjugate of the latter process was calculated within the Born-Oppenheimer approximation by Bates already in 1953 [145,146], with a fully nonadiabatic treatment [147] available 60 years later. Vibrationally resolved photoionization cross sections have also recently been calculated by Singor *et al.* [148]. From energy considerations only, the minimum photon energy required to drive dissociative ionization from the rovibrational ground state is 16.2 eV, but the cross section is still minuscule up to about 25 eV and remains small for energies below 30 eV. The reason is that one needs to account for the threshold energy of the Franck-Condon envelope. For the equilibrium separation of H_2^{+} ($\sim 2\,a_0$) the minimum photon energy is $\sim$30 eV, at which point the cross section goes through a maximum of $\sim 6.5\times10^{-19}\ \mathrm{cm}^2$.

Similarly to the analysis of reaction R.8, we use the principle of detailed balance to relate the electronic ground-state

photodissociative-ionization rate coefficient, $\alpha^{\rm PDI}_{l\to u}(T)$, to the reverse radiative association recombination rate coefficient (units of $\rm cm^6 s^{-1}$), $\alpha^{\rm RAR}_{u\to l}(T)$, via

$$\alpha^{\rm RAR}_{u\to l}(T) = 7.050\times10^{-49}\frac{g_{{\rm W}l}}{g_{{\rm X}u'}g_{{\rm Y}u''}}e^{E_0/k_BT}\left(\frac{\rm Da\,eV}{\mu_{\rm XY}k_BT}\right)^{3/2} \times \alpha^{\rm PIDE}_{l\to u}(T), \tag{10}$$

where $g_{{\rm W}l}$ is the statistical weight of the molecule, $g_{{\rm X}u'}$ and $g_{{\rm Y}u''}$ are the statistical weights of the ions, $\mu_{\rm XY}$ is the reduced mass of the products X and Y (in units of daltons), and E_0 is the threshold energy for the dissociative-ionization process. Here we included stimulated emission and assumed Maxwellian and Planck distributions for all the respective particles and that they are all the same temperature, i.e., $T \equiv T_{\overline{p}} = T_e = T_\gamma$. The total rate, $\lambda^{\rm RAR}$, of $\overline{\rm H}_2^-$ is $\lambda^{\rm RAR} = \sum_l \alpha^{\rm RAR}_{u\to l}(T) n_e$ per $\overline{p}$ squared. Using the cross sections of Singor *et al.* [148], we estimated the total rate coefficient summing over all $v = 0$–19 states of the H_2^+ electronic ground state. For the 5–30 K range this rate coefficient is numerically zero in a double-precision calculation. Investigating this total rate coefficient over a range of higher temperatures it peaks at approximately 10^{-39} $\rm cm^6\,s^{-1}$. Hence, this reaction is likely not feasible since competing production (for instance via radiative recombination, reaction R.2) of $\overline{\rm H}$s would likely deplete the trap of the e^+s and $\overline{p}$s.

3. Reaction R.10: $\overline{p} + \overline{\rm H} \leftrightarrow \gamma + \overline{\rm H}_2^-$

This radiative association (RA) reaction has been treated extensively by Zammit and coworkers [47], who provided cross sections and rate coefficients for the process for $\overline{\rm H}$ in principal quantum numbers 1–3 and for temperatures in the range 10^{-3}–10^5 K. The cross sections for the excited states of $\overline{\rm H}$ were found to be 10^5–10^6 times greater than those for the ground state, an increase that was passed over to the rate coefficients. Below roughly 1 K, the excited states rate coefficients were in the range between $\alpha^{\rm RA} = 10^{-13}$–$10^{-16}$ $\rm cm^3\,s^{-1}$ and to increase with antihydrogen temperature as $T_{\overline{\rm H}}^{-0.5}$. The interested reader is referred to Ref. [47], and to the discussion of experimental considerations which is included there. It may be possible to laser stimulate this process, but to the best of our knowledge, this has not been considered previously.

4. Reaction R.11: $\overline{\rm H}^* + \overline{\rm H} \leftrightarrow e^+ + \overline{\rm H}_2^-$

Associative ionization (AI) can also occur in collisions between neutrals (nAI). Unlike reaction R.12 this reaction is endothermic for $n_{\overline{\rm H}} \leqslant 2$.

We first consider the case $n_{\overline{\rm H}} = 2$. This channel has a threshold of about 0.75 eV. Urbain *et al.* [149] have experimentally (& theoretically) studied the H + H AI reaction, finding that whereas the highly exothermic ionic case (reaction R.12) is completely dominated by the Coulombic interaction and thus provides little insight into the reaction mechanisms, the simplest neutral H(1*S*) + H(2*S*) collisions allow careful quantal treatment of the dynamics. Limiting their theoretical studies to a minimal number of potential energy curves (electronic states) with a 0.75 eV threshold (the threshold energy for the reaction), comparisons have been made to experimentally determined absolute cross sections for the relative energy range 0.5–10 eV. The cross section peaks at 3.4 eV (where the H_2^+ dissociation channel opens), where its value is $2.4\times10^{-17}\,\rm cm^2$. Above this energy the dissociation of the ion becomes competitive.

These measurements enabled Rawlings *et al.* [150] to calculate rate coefficients for H(2*S*) and H(2*P*), giving $\alpha^{\rm nAI} = 2.41\times10^{-9}(T_{\overline{\rm H}}/\rm K)^{-0.35}\exp(-17829/[T_{\overline{\rm H}}/\rm K])$ $\rm cm^3\,s^{-1}$ for the weighted *S* and *P* substates. Due to the 0.75 eV threshold of the reaction, the direct radiative association reaction to form $\overline{\rm H}_2$ (reaction R.13) is likely competitive at temperatures $\lesssim$6000 K, but here the rate for AI grows rapidly, from 3.3×10^{-12} $\rm cm^3\,s^{-1}$ at 4000 K to 1.61×10^{-11} $\rm cm^3\,s^{-1}$ at 10 000 K thus likely overtaking the radiative process.

Theoretical cross sections for associative ionization from the H(1*S*) + H(2*S*) channel were recently published by Hörnquist *et al.* [151]. These results are also in reasonably good agreement with the measurements by Urbain *et al.* [149] in the relative energy range 0.001–3 eV, though at energies above ∼3 eV the measured cross section is underestimated. This could be due to molecular states that were not included in the calculation. For low energies the results agree well with the rate coefficient calculated from these data, which is well fitted by $\alpha^{\rm nAI} = 1.72\times10^{-9}(T_{\overline{\rm H}}/\rm K)^{-0.44}\exp(-14950/[T_{\overline{\rm H}}/\rm K])$ $\rm cm^3 s^{-1}$ for $T_{\overline{\rm H}} < 10^4$ K [122]. Thus, as the temperature crosses the temperature equivalent of the energy of the formation threshold (8800 K), the theoretical rate coefficient increases from zero somewhat faster than the measured one.

We now turn to states with $n_{\overline{\rm H}} > 2$. Brouillard and Urbain [152] extended their measurements to include the 3*S* and 4*S* states for energies ranging from 5 meV to 4 eV (for 3*S*, see also Ref. [153]). Unlike for $n_{\overline{\rm H}} = 1, 2$, the 3*S* channel is exothermic by about 1.13 eV. At energies below 0.1 eV, the cross section was found to vary as $\sim2\times10^{-17}(E/\rm eV)^{-1}\,cm^2$, thus *not* following the Wigner law. This energy dependence was attributed to a limit imposed by the requirement that the rotational energy of the molecular ion formed must be less than its dissociation energy [153]. At 0.1 eV the cross section levels out at $\sim2\times10^{-16}\,\rm cm^2$, with some oscillations arising from interfering reaction paths. Above ∼1.6 eV the cross section drops rapidly because the (atomic) ionization channel opens.

A recent fully quantum mechanical calculation [151] gives good agreement with experiments in the low-energy region. However, the cross section shows large oscillations, arising through interferences between different pathways though the potential energy landscape, which makes it difficult to deduce its overall energy dependence. At higher energies ($\gtrsim$0.1 eV) the results show the same features as the measurements in Ref. [153], though the values are consistently significantly smaller.

Turning to the 4*S* state, the reaction is exothermic by 1.79 eV. The cross section has a similar energy dependence as the 3*S* state, though at energies below ∼1 eV it is larger by a factor ∼2–3 (again with the $1/E$ dependence) [152]. In this case theory does not reproduce the low-energy $1/E$ dependence observed in experiments and again underestimates the measurements at higher energies [151]. An interesting feature of the calculations is that while the 3*S* low-energy cross section is dominated by singlet states, the 4*S* cross section mainly

relies on triplet states. This has implications for experiments using magnetically trapped antihydrogen.

The low-energy rate coefficients based on the cross sections from Ref. [151] are roughly constant, where at $T = 1$ K $\alpha^{\mathrm{nAI}} = 9 \times 10^{-11}$ cm^3 s^{-1} for the $3S$ state and $\alpha^{\mathrm{nAI}} = 5 \times 10^{-10}$ cm^3 s^{-1} for the $4S$ state. This is lower than for the ionic channel, reaction R.12, but has the advantage that it does not require the atomic ion $\overline{\mathrm{H}}^+$. On the other hand, maintaining a population of $3S$ or $4S$ excited $\overline{\mathrm{H}}$ is also an experimental challenge.

Zammit *et al.* proposed the doubly excited AI reaction $\overline{\mathrm{H}}(2S) + \overline{\mathrm{H}}(2S) \rightarrow \overline{\mathrm{H}}_2^- + e^+$ as a promising route to formation of the $\overline{\mathrm{H}}_2^-$ ion [47]. The scheme involved exciting $\overline{\mathrm{H}}$ trapped in a shallow magnetic trap. The low magnetic fields are necessary to minimize losses due to mixing of the $2S$ and $2P$ states of $\overline{\mathrm{H}}$ from the motional $\mathbf{v} \times \mathbf{B}$ electric field, with subsequent fast spin-flip decay to an untrapped substate of $\overline{\mathrm{H}}(1S)$. Assuming a $\overline{\mathrm{H}}(2S)$ density of 10^3 cm^{-3} at a temperature of 1 mK filling a trap volume of 10 cm^3 a reaction rate 10^{-2} s^{-1} was obtained. Since then laser cooling of antihydrogen has been demonstrated [17], which adds credibility to the scheme.

The estimates in Ref. [47] were based on cross sections for AI and the competing Penning ionization (PI) process $[\overline{\mathrm{H}}(2S) + \overline{\mathrm{H}}(2S) \rightarrow \overline{\mathrm{H}}(1S) + \overline{p} + e^+]$ obtained from calculations of the total ionization cross section at low energies [154], with the relative contributions given by a fit to the higher energy data calculated in Ref. [155]. Recently, Taylor *et al.* [156] refined the low-energy calculations of this and competing processes, by including the splittings due to fine structure and the Lamb shift. They found that, contrary to the expectations in Ref. [47], PI dominates over AI at all energies. Furthermore, the double excitation transfer (DET) process $\overline{\mathrm{H}}(2S) + \overline{\mathrm{H}}(2S) \rightarrow \overline{\mathrm{H}}(2P) + \overline{\mathrm{H}}(2P)$ was found to dominate over AI down to sub-millikelvin temperatures. At 1 mK the rate coefficient for AI was found to be $\sim 2 \times 10^{-9}$ cm^3 s^{-1}, while for PI and DET both $\sim 5 \times 10^{-9}$ cm^3 s^{-1}. At lower temperatures DET drops sharply, while AI and PI remain roughly constant. The estimates in Ref. [47] should be revisited in the light of these new data.

A lot of experimental and theoretical work has been done on the reverse, dissociative recombination, reaction, though mostly for the HD^+ isotope. Recently Hörnquist *et al.* published calculations also for this process [157] (see also references in this paper). The total rate coefficients for dissociative recombination at meV energies and below are 10^{-8}–10^{-7} cm^3 s^{-1}.

5. Reaction R.12: $\overline{p} + \overline{\mathrm{H}}^+ \leftrightarrow e^+ + \overline{\mathrm{H}}_2^-$

Associative ionization is the most basic mechanism to form molecular bonds, with the colliding species transferring energy to the ejected positron/electron. This AI reaction between charged species is exothermic by about 2 eV. The cross section has been measured by Poulaert *et al.* [158] in the relative energy, E, range 0.001–3 eV. At 0.003 eV the cross section was found to be $\sim 1.5 \times 10^{-14}$ cm^2. According to the Wigner law this cross section is proportional to $1/E$ at low collision energies, and hence the collision rate grows as $1/\sqrt{E}$ as E is lowered. Based on this measurement, Galli and Palla [68] (see Table I of that article) fitted values for the reaction rate at associated temperatures above and below 8000 K. For the latter $\alpha^{\mathrm{AI}} \approx 7 \times 10^{-9} (T/\mathrm{K})^{-0.35}$ cm^3 s^{-1}.

A theoretical calculation by Urbain *et al.* [159] gave good agreement with the experimental results, especially below 0.1 eV where $\sigma^{\mathrm{AI}} \simeq 5 \times 10^{-17} (E/\mathrm{eV})^{-1}$ cm^2, while at higher energies it slightly underestimated the cross section. A more recent calculation gives a cross section larger by a factor ~ 2 in the low-energy limit, and confirmed the $1/E$ scaling at low energies [151]. The rate coefficient calculated from these data is well fitted by the expression $\alpha^{\mathrm{AI}} \approx 2.5 \times 10^{-8} \times (T/\mathrm{K})^{-0.5}$ cm^3 s^{-1} in the temperature range 1 to 100 K. This is consistent with the Wigner law, and hence the rate coefficient can be expected to have the same form also for lower energies [122].

Thus, observation of this reaction may be feasible with current/near-future $\overline{p}$ clouds, though noting the major difficulty lies in producing (and trapping) the anti-ions, as described more fully in Sec. IV B.

This reaction was suggested by Myers [45] as a way to form the $\overline{\mathrm{H}}_2^-$ ion. However, he also noted that it competes unfavorably with the alternative final channel $\overline{\mathrm{H}} + \overline{\mathrm{H}}$ (cf. reaction R.5). Indeed, at low energies both cross sections vary as $1/E$, but with a larger coefficient for the mutual neutralization process.

D. Group D: $\overline{\mathrm{H}}_2$ formation

Here a selection of reactions leading to the formation of the antihydrogen molecule, $\overline{\mathrm{H}}_2$, are discussed.

1. Reaction R.13: $\overline{\mathrm{H}}^* + \overline{\mathrm{H}} \leftrightarrow \gamma + \overline{\mathrm{H}}_2$

Classically, radiative association, of which this reaction is a typical example, is inefficient and only proceeds if a strong electronic transition is available within the product molecule. This transition enables the emission of a stabilizing photon and hence enhances the radiative association rate. Latter and Black [160] semiclassically calculated the radiative rate coefficient for the ground state and first excited state reaction of neutral H as $\alpha^{\mathrm{RA}} \sim (1\text{-}3) \times 10^{-14}$ cm^3 s^{-1} for 50 K. In this calculation, ground-state rates are considered negligible due to the absence of stabilizing transitions and dipole transitions are forbidden, and simplifying assumptions such as the absence of low temperature effects (e.g., tunneling and shape resonances) are employed. Thus, despite the tantalizing higher and increasing rate at lower temperatures for the experimentally convenient $\overline{\mathrm{H}}(n_{\overline{\mathrm{H}}} = 2)$ state, extrapolation to lower temperatures is not advised. Given this rate coefficient, it is worthwhile to consider this reaction along with the competing reaction R.11 (followed by reaction R.20), and we note that in vacuum (i.e., without surface catalysis) other "standard" gas-phase routes (some of which have been discussed in this paper) will likely dominate.

2. Reaction R.14: $e^+ + \overline{\mathrm{H}} + \overline{\mathrm{H}} \leftrightarrow e^+ + \overline{\mathrm{H}}_2$

Similarly to reaction R.8, the three-body association of $\overline{\mathrm{H}}_2$ can proceed via the reverse of positron-impact

dissociation of $\overline{\mathrm{H}}_2$. Since this interaction proceeds predominately through the exchange interaction (i.e., $b^3\Sigma_u^+ \leftrightarrow X^1\Sigma_g^+$ transitions), an electron collision partner is not considered here since an exchange transition is not possible. The matter counterpart, electron-impact dissociation of H_2 into H ground-state products has been studied extensively. However, recent CCC calculations [137,161–166] predicted errors with previous calculations and experiments, which for the integrated cross sections, were subsequently confirmed by experiment [167] and other close-coupling calculations [168] (for further details see the discussions in Refs. [162,163,166,167]). As we did for reaction R.8, we evaluate the total three-body association rate coefficient for interacting ground-state $\overline{\mathrm{H}}$s using the fitted cross sections of Scarlett *et al.* [169,170]. Between 5 and 30 K, the total three-body association rate coefficient is approximately 10^{-35}–10^{-34} $\mathrm{cm}^6\,\mathrm{s}^{-1}$, hence a total rate $\lambda^{3\mathrm{BA}} \approx 10^{-27}$–$10^{-26}\mathrm{cm}^3\,\mathrm{s}^{-1}$ per $\overline{\mathrm{H}}$ squared, when setting $n_e \sim 10^8$ cm^{-3}. Hence, this reaction seems unlikely for the near-term positron and $\overline{\mathrm{H}}$ trapping and production capabilities.

3. Reaction R.15: $\bar{p} + \overline{\mathrm{H}}^+ \leftrightarrow \gamma + \overline{\mathrm{H}}_2$

Particularly at low energies, this reaction is of limited, e.g., astrophysical, relevance and as such has garnished little attention, resulting in no relevant calculations to date. Though the approximately 17 eV [171] energy available is favorable for the radiative association reaction (via the $F^1\Sigma_g^+ \rightarrow X^1\Sigma_g^+$ transition), owing to $\overline{\mathrm{H}}_2$ parity requirements a second-order elimination E2-type reaction is required for a transition directly to the ground state, which is expected to result in a very low production rate. Production of $\overline{\mathrm{H}}_2^*$ allows for a two-step E1-type reaction which, while potentially allowing for radiative decay to the ground state, also opens loss-inducing dissociation channels. Considering the need of $\overline{\mathrm{H}}^+$ and second-order or indirect processes, this reaction seems unlikely with near-term capabilities.

4. Reactions R.16 to R.20:

Of these processes, we do not discuss reaction R.17 further: Though it is likely to proceed efficiently, the combined difficulty of creating $\overline{\mathrm{H}}^+$ and $\overline{\mathrm{H}}_2^-$ means that it is not currently worthwhile to consider its experimental feasibility.

The three-body reaction (number R.18) to create $\overline{\mathrm{H}}_2$ is likely to proceed rapidly at the values of n_e and T_e currently available, in conditions similar to those discussed regarding $\overline{\mathrm{H}}$ formation via reaction R.1: once $\overline{\mathrm{H}}_2^-$ has been created and isolated. Neutralization of the latter would produce the untrapped molecule with a distinctive double $\bar{p}$ annihilation signal.

Matter equivalents of reactions R.16, R.19, and R.20 are discussed in Galli and Palla [68], and all are experimentally difficult due to their involvement of $\overline{\mathrm{H}}^+$ or $\overline{\mathrm{H}}_2^-$. Reaction R.16 (associative detachment) data agree at temperatures below 10^3 K with a rate coefficient around 10^{-9} $\mathrm{cm}^3\,\mathrm{s}^{-1}$ (requiring $\overline{\mathrm{H}}^+$). Reaction R.19 has been assigned a temperature-independent (Langevin) rate of around 6.4×10^{-10} $\mathrm{cm}^3\,\mathrm{s}^{-1}$ (requiring $\overline{\mathrm{H}}_2^-$) derived from a 300 K measurement of Karpas *et al.* [172]. Finally, reaction R.20 has been represented by its reverse in Ref. [68], based on the work of O'Neil and Reinhardt [173] although no information is available for the forward reaction: though, similarly to reaction R.18, once $\overline{\mathrm{H}}_2^-$ has been created and isolated the reaction will likely proceed readily due to the two-body nature of the reactants.

E. Group E: $\overline{\mathrm{H}}_3^-$ formation

The formation of the antihydrogen molecular anion $\overline{\mathrm{H}}_3^-$ via reactions R.21 and R.22 is also considered experimentally very difficult in the near term, and we offer no further discussion here.

F. Group F: $\overline{\mathrm{H}}$ destruction

Reaction R.23 is an important process between excited $\overline{\mathrm{H}}$ atoms, which can lead to the depletion of a trapped antiatom sample. This Penning ionization process was treated in detail in Ref. [47] (to which the interested reader is referred), where it was found that reaction rates were comparable to the $\overline{\mathrm{H}}_2^-$ formation reactions R.10 and R.11. Since the study of Ref. [47], Taylor *et al.* [156] updated these low-energy calculations, as discussed for reaction R.11.

V. SUMMARY

We have presented an overview of antimatter reactions, as encapsulated by the bubble diagram shown in Fig. 1, leading to the formation of antihydrogen atoms and species containing more antiparticles, such as $\overline{\mathrm{H}}^+$ and $\overline{\mathrm{H}}_2^-$. Many of the reactions have been discussed, either in terms of published work explicitly relating to theory and/or simulations of antimatter or based on data available from theory and experiment for the relevant matter systems counterpart (including time-reversed processes).

Our study has been stimulated, as discussed in Sec. II, by experimental achievements in which antihydrogen has been stacked and stored in a magnetic minimum trap with a lifetime against loss of several tens of hours. This, together with the low confinement temperatures and the antiatom densities which seem feasible in the near future, and with advances in manipulation of the antiatom states and the advent of laser and adiabatic cooling, has brought the prospect of antihydrogen chemistry within sight.

We have endeavoured to evaluate most of the reactions shown in Fig. 1 to provide a rating for the information available, together with the likelihood of experimental progress, as shown in Table I. Our aim has been to identify processes that are of potential near-future interest, in particular for the production of new antimatter systems, and which would benefit from further study. We anticipate new theoretical calculations and simulations (using new or existing data) to further assess feasibility of the production of new species.

ACKNOWLEDGMENTS

The authors thank Dr. Christopher Fontes for useful discussions, Professor Jack Straton for providing the details of Dr C. M. Keating's thesis (see Ref. [114]), and Dr. Johan

Hörnquist and Professor Åsa Larson for providing unpublished data. C.J.B., S.E., and M.C. are grateful to the EPSRC (UK) for their support of the antimatter research programme at Swansea. S.J. acknowledges support from the Swedish Research Council (VR), grant 2021-04005. M.C.Z. would like to specifically acknowledge the support of the Los Alamos National Laboratory's (LANL) Laboratory Directed Research and Development program Project No. 20240391ER and the ASC PEM Atomic Physics Project. LANL is operated by Triad National Security, LLC, for the National Nuclear Security Administration of the U.S. Department of Energy under Contract No. 89233218NCA000001.

APPENDIX: ALTERNATIVE REACTIONS

In Table II we present a set of typically higher-order/less-probable reactions which may contribute to the formation of the antimatter bound states discussed in the previous sections. It is likely that some information exists from the matter counterparts of these processes in order to make estimates for rates. They are given here to illustrate the potential richness of antihydrogen chemistry. Further work is necessary to judge which, if any, of these processes may prove to be experimentally feasible in the not-too-distant future. For example, the reverse of several of these reactions involve two-positron processes, which are known to have relatively small cross sections for few-electron systems; e.g., electron-impact double ionization cross section of He [174] (A.11).

We note that the double spontaneous radiative recombination (A.6) was searched for at CRYRING by Schuch *et al.* [175]. The rate coefficient was measured as $\alpha^{\mathrm{2SRR}} = (2.1 \pm 0.8) \times 10^{-19}\ \mathrm{cm^3\,s^{-1}}$ and thus consistent with zero. Unfortunately, however, it appears that the quoted rate coefficient has incorrect units (since this is a three-body, not a two-body, process). Using the parameters from Ref. [175], we instead obtain $\alpha^{\mathrm{2SRR}} = (7.0 \pm 2.7) \times 10^{-27}\ \mathrm{cm^6\,s^{-1}}$.

We have also reevaluated the form of rate coefficient based on MR of the reverse reaction (double photoionization), which at low energies was found to follow the Wannier threshold law by Kheifets and Bray [176], as

$$\alpha_{fi}^{\mathrm{2SRR,2D}}(T_\perp) = \frac{h^3\sigma_0}{32\pi m_e^3 c^2}\left(\frac{k_B T_\perp}{1\ \mathrm{eV}}\right)^a \left(\frac{E_{\mathrm{ion}}}{k_B T_\perp}\right)^2 \Gamma(a), \quad \text{(A1)}$$

where $T_\perp$ is the transverse temperature of the electrons in the beam, E_{ion} is the double ionization energy of H^-, $a = 1.127$ (as dictated by the Wannier law), and $\sigma_0 = 9.5 \times 10^{-20}\ \mathrm{cm^2}$. Using this expression and the parameters from Ref. [175], we arrive at a rate coefficient $\sim 4 \times 10^{-36}\ \mathrm{cm^6\,s^{-1}}$. This is many orders of magnitude below what could reasonably be measured, and of very little consequence for antihydrogen chemistry.

TABLE II. Antihydrogen chemistry reactions.

	Reactions
	Group A: $\overline{\mathrm{H}}$ formation
(A.2)	$e^+ + \overline{p} + \overline{p} \leftrightarrow \overline{p} + \overline{\mathrm{H}}$
	Group B: $\overline{\mathrm{H}}^+$ formation
(A.3)	$e^+ + \overline{p} + \overline{\mathrm{H}} \leftrightarrow \overline{p} + \overline{\mathrm{H}}^+$
(A.4)	$e^+ + \mathrm{Ps} + \overline{p} \leftrightarrow e^- + \overline{\mathrm{H}}^+$
(A.5)	$e^+ + \mathrm{Ps} + \overline{\mathrm{H}} \leftrightarrow \mathrm{Ps} + \overline{\mathrm{H}}^+$
(A.6)	$e^+ + e^+ + \overline{p} \leftrightarrow \gamma + \overline{\mathrm{H}}^+$
(A.7)	$e^+ + e^+ + e^+ + \overline{p} \leftrightarrow e^+ + \overline{\mathrm{H}}^+$
	Group C: $\overline{\mathrm{H}}_2^-$ formation
(A.8)	$\mathrm{Ps} + \overline{p} + \overline{p} \leftrightarrow e^- + \overline{\mathrm{H}}_2^-$
(A.9)	$\overline{p} + \overline{\mathrm{H}} + \overline{\mathrm{H}} \leftrightarrow \overline{\mathrm{H}} + \overline{\mathrm{H}}_2^-$
(A.10)	$\mathrm{Ps} + \overline{p} + \overline{\mathrm{H}} \leftrightarrow \mathrm{Ps} + \overline{\mathrm{H}}_2^-$
(A.11)	$e^+ + e^+ + \overline{p} + \overline{p} \leftrightarrow e^+ + \overline{\mathrm{H}}_2^-$
(A.12)	$\overline{p} + \overline{p} + \overline{\mathrm{H}} \leftrightarrow \overline{p} + \overline{\mathrm{H}}_2^-$
(A.13)	$e^+ + \overline{p} + \overline{p} + \overline{p} \leftrightarrow \overline{p} + \overline{\mathrm{H}}_2^-$
	Group D: $\overline{\mathrm{H}}_2$ formation
(A.14)	$\mathrm{Ps}^* + \overline{\mathrm{H}}_2^- \leftrightarrow e^- + \overline{\mathrm{H}}_2$
(A.15)	$\overline{p} + \overline{\mathrm{H}} + \overline{\mathrm{H}} \leftrightarrow \overline{p} + \overline{\mathrm{H}}_2$
(A.16)	$\overline{\mathrm{H}} + \overline{\mathrm{H}} + \overline{\mathrm{H}} \leftrightarrow \overline{\mathrm{H}} + \overline{\mathrm{H}}_2$
(A.17)	$e^+ + e^+ + \overline{p} + \overline{\mathrm{H}} \leftrightarrow e^+ + \overline{\mathrm{H}}_2$
(A.18)	$e^+ + e^+ + e^+ + \overline{p} + \overline{p} \leftrightarrow e^+ + \overline{\mathrm{H}}_2$
(A.19)	$e^+ + e^+ + \overline{p} + \overline{p} \leftrightarrow \gamma + \overline{\mathrm{H}}_2$
(A.20)	$\mathrm{Ps}^* + \overline{p} + \overline{\mathrm{H}} \leftrightarrow e^- + \overline{\mathrm{H}}_2$
(A.21)	$e^+ + \mathrm{Ps}^* + \overline{p} + \overline{p} \leftrightarrow e^- + \overline{\mathrm{H}}_2$
(A.22)	$e^+ + \overline{p} + \overline{\mathrm{H}}_2^- \leftrightarrow \overline{p} + \overline{\mathrm{H}}_2$
(A.23)	$e^+ + \overline{p} + \overline{p} + \overline{\mathrm{H}} \leftrightarrow \overline{p} + \overline{\mathrm{H}}_2$
(A.24)	$e^+ + e^+ + \overline{p} + \overline{p} + \overline{p} \leftrightarrow \overline{p} + \overline{\mathrm{H}}_2$

[1] W. A. Bertsche, E. Butler, M. Charlton, and N. Madsen, J. Phys. B: At. Mol. Opt. Phys. **48**, 232001 (2015).
[2] M. Amoretti *et al.* (ATHENA Collaboration), Nature (Lond.) **419**, 456 (2002).
[3] G. Gabrielse *et al.* (ATRAP Collaboration), Phys. Rev. Lett. **89**, 213401 (2002).
[4] G. B. Andresen *et al.* (ALPHA Collaboration), Nature (Lond.) **468**, 673 (2010)
[5] G. B. Andresen *et al.* (ALPHA Collaboration), Phys. Lett. B **695**, 95 (2011).
[6] G. B. Andresen *et al.* (ALPHA Collaboration), Nat. Phys. **7**, 558 (2011).

[7] G. Gabrielse, R. Kalra, W. S. Kolthammer, R. McConnell, P. Richerme, D. Grzonka, W. Oelert, T. Sefzick, M. Zielinski, D. W. Fitzakerley, M. C. George, E. A. Hessels, C. H. Storry, M. Weel, A. Mullers, and J. Walz (ATRAP Collaboration), Phys. Rev. Lett. **108**, 113002 (2012).

[8] M. Ahmadi *et al.* (ALPHA Collaboration), Nat. Commun. **8**, 681 (2017).

[9] C. Amole *et al.* (ALPHA Collaboration), Nature (Lond.) **483**, 439 (2012).

[10] C. Amole *et al.* (ALPHA Collaboration), Nat. Commun. **5**, 3955 (2014).

[11] M. Ahmadi *et al.* (ALPHA Collaboration), Nature (Lond.) **529**, 373 (2016).

[12] M. Ahmadi *et al.* (ALPHA Collaboration), Nature (Lond.) **548**, 66 (2017).

[13] M. Ahmadi *et al.* (ALPHA Collaboration), Nature (Lond.) **541**, 506 (2017).

[14] M. Ahmadi *et al.* (ALPHA Collaboration), Nature (Lond.) **557**, 71 (2018).

[15] M. Ahmadi *et al.* (ALPHA Collaboration), Nature (Lond.) **561**, 211 (2018).

[16] M. Ahmadi *et al.* (ALPHA Collaboration), Nature (Lond.) **578**, 375 (2020).

[17] C. J. Baker *et al.* (ALPHA Collaboration), Nature (Lond.) **592**, 35 (2021).

[18] E. K. Anderson *et al.* (ALPHA Collaboration), Nature (Lond.) **621**, 716 (2023).

[19] F. Robicheaux, J. Phys. B: At. Mol. Opt. Phys. **41**, 192001 (2008).

[20] D. Vrinceanu, B. E. Granger, R. Parrott, H. R. Sadeghpour, L. Cederbaum, A. Mody, J. Tan, and G. Gabrielse, Phys. Rev. Lett. **92**, 133402 (2004).

[21] F. Robicheaux and J. D. Hanson, Phys. Rev. A **69**, 010701(R) (2004).

[22] T. Pohl, H. R. Sadeghpour, and G. Gabrielse, Phys. Rev. Lett. **97**, 143401 (2006).

[23] E. M. Bass and D. H. E. Dubin, Phys. Plasmas **16**, 012101 (2009).

[24] B. Radics, D. J. Murtagh, Y. Yamazaki, and F. Robicheaux, Phys. Rev. A **90**, 032704 (2014).

[25] S. Jonsell, D. P. van der Werf, M. Charlton, and F. Robicheaux, J. Phys. B: At. Mol. Opt. Phys. **42**, 215002 (2009).

[26] S. Jonsell, M. Charlton, and D. P. van der Werf, J. Phys. B: At. Mol. Opt. Phys. **49**, 134004 (2016).

[27] S. Jonsell and M. Charlton, New J. Phys. **20**, 043049 (2018).

[28] S. Jonsell and M. Charlton, New J. Phys. **21**, 073020 (2019).

[29] S. Jonsell and M. Charlton, J. Phys. B: At. Mol. Opt. Phys. **54**, 025001 (2021).

[30] C. Amole *et al.* (ALPHA Collaboration), Nucl. Instrum. Methods A **735**, 319 (2014).

[31] M. Charlton, S. Eriksson and G. Shore, *Antihydrogen and Fundamental Physics*, Springer Briefs in Physics (Springer International, New York, 2020), p. 95.

[32] V. A. Kostelecký and A. J. Vargas Phys. Rev. D **92**, 056002 (2015).

[33] V. A. Kostelecký and A. J. Vargas, Phys. Rev. D **98**, 036003 (2018).

[34] C. J. Baker *et al.* (ALPHA Collaboration), Nat. Phys. **21**, 201 (2025).

[35] C. G. Parthey, A. Matveev, J. Alnis, B. Bernhardt, A. Beyer, R. Holzwarth, A. Maistrou, R. Pohl, K. Predehl, T. Udem, T. Wilken, N. Kolachevsky, M. Abgrall, D. Rovera, C. Salomon, P. Laurent, and T. W. Hänsch, Phys. Rev. Lett. **107**, 203001 (2011).

[36] C. Carli, D. Gamba, C. Malbrunot, L. Ponce, and S. Ulmer, Nucl. Phys. News **32**, 21 (2022).

[37] N. Kuroda *et al.*, Nat. Commun. **5**, 3089 (2014).

[38] M. Diermaier *et al.*, Nat. Commun. **8**, 15749 (2017).

[39] C. Amsler *et al.* (AEgIS Collaboration), Commun. Phys. **4**, 19 (2021).

[40] P. Adrich *et al.* (GBAR Collaboration), Eur. Phys. J. C **83**, 1004 (2023).

[41] J. Walz and T. W. Hänsch, Gen. Relativ. Gravit. **36**, 561 (2004)

[42] C. M. Keating, M. Charlton, and J. C. Straton, J. Phys. B: At. Mol. Opt. Phys. **47**, 225202 (2014).

[43] C. M. Keating, K. Y. Pak, and J. C. Straton, J. Phys. B: At. Mol. Opt. Phys. **49**, 074002 (2016).

[44] A. Jacob, S. F. Zhang, C. Müller, X. Ma, and A. B. Voitkiv, Phys. Rev. Res. **2**, 013105 (2020).

[45] E. G. Myers, Phys. Rev. A **98**, 010101 (2018).

[46] E. G. Myers, Hyperfine Interact. **239**, 43 (2018).

[47] M. C. Zammit *et al.*, Phys. Rev. A **100**, 042709 (2019).

[48] S. Schiller, Contemp. Phys. **63**, 247 (2022).

[49] G. M. Shore, arXiv:2412.09730.

[50] M. Ahmadi, B. X. R. Alves, C. J. Baker, W. Bertsche, A. Capra, C. Carruth, C. L. Cesar, M. Charlton, S. Cohen, R. Collister, S. Eriksson, A. Evans, N. Evetts, J. Fajans, T. Friesen, M. C. Fujiwara, D. R. Gill, J. S. Hangst, W. N. Hardy, M. E. Hayden, C. A. Isaac, M. A. Johnson, S. A. Jones, S. Jonsell, L. Kurchaninov, N. Madsen, M. Mathers, D. Maxwell, J. T. K. McKenna, S. Menary, T. Momose, J. J. Munich, K. Olchanski, A. Olin, P. Pusa, C. O. Rasmussen, F. Robicheaux, R. L. Sacramento, M. Sameed, E. Sarid, D. M. Silveira, C. So, G. Stutter, T. D. Tharp, J. E. Thompson, R. I. Thompson, D. P. vanderWerf, and J. S. Wurtele (ALPHA Collaboration), Phys. Rev. Lett. **120**, 025001 (2018).

[51] F. Robicheaux, Phys. Rev. A **73**, 033401 (2006).

[52] T. Topçu and F. Robicheaux, Phys. Rev. A **73**, 043405 (2006).

[53] M. Sameed, D. Maxwell, and N. Madsen, New J. Phys. **22**, 013009 (2020).

[54] C. J. Baker *et al.* (ALPHA Collaboration), Nat. Commun. **12**, 6139 (2021).

[55] B. M. Jelenković, A. S. Newbury, J. J. Bollinger, W. M. Itano, and T. B. Mitchell, Phys. Rev. A **67**, 063406 (2003).

[56] N. Madsen, F. Robicheaux, and S. Jonsell, New J. Phys. **16**, 063046 (2014).

[57] S. Maury, Hyperfine Interact. **109**, 43 (1997).

[58] P. Belochitskii, T. Eriksson, and S. Maury, Nucl. Instrum. Methods B **214**, 176 (2004).

[59] G. Gabrielse, X. Fei, K. Helmerson, S. L. Rolston, R. Tjoelker, T. A. Trainor, H. Kalinowsky, J. Haas, and W. Kells, Phys. Rev. Lett. **57**, 2504 (1986).

[60] X. Feng, M. H. Holzscheiter, M. Charlton, J. Hangst, N. S. P. King, R. A. Lewis, Rochet J and Y. Yamazaki, Hyperfine Interact. **109**, 145 (1997).

[61] J. R. Danielson, D. H. E. Dubin, R. G. Greaves, and C. M. Surko, Rev. Mod. Phys. **87**, 247 (2015).

[62] J. Fajans and C. M. Surko, Phys. Plasmas **27**, 030601 (2020).

[63] S. Maury *et al.* Hyperfine Interact. **229**, 105 (2014).

[64] W. Bartmann *et al.* (on behalf of the ELENA and AD teams), Phil. Trans. R. Soc. A. **376**, 20170266 (2018).

[65] A. Husson *et al.* (GBAR Collaboration), Nucl. Instrum. Methods A **1002**, 165245 (2021).

[66] P. H. Donnan, M. C. Fujiwara, and F. Robicheaux, J. Phys. B: At. Mol. Opt. Phys. **46**, 025302 (2013).

[67] S. Lepp, P. C. Stancil, and A. Dalgarno, J. Phys. B: At. Mol. Opt. Phys. **35**, R57 (2002).

[68] D. Galli and F. Palla, Astron. Astrophys. **335**, 403 (1998).

[69] P. C. Stancil and A. Dalgarno, Faraday Discuss. **109**, 61 (1998).

[70] M. M. Michaelis and R. Bingham, Laser Part. Beams **6**, 83 (1988).

[71] M. M. Nieto, M. H. Holzscheiter, and T. J. Phillips, J. Opt. B: Quantum Semiclassic. Opt. **5**, S547 (2003).

[72] M. E. Glinsky and O'T. M. Neil, Phys. Fluids B **3**, 1279 (1991).

[73] B. Makin and J. C. Keck, Phys. Rev. Lett. **11**, 281 (1963).

[74] P. Mansbach and J. Keck, Phys. Rev. **181**, 275 (1969).

[75] F. Robicheaux, Phys. Rev. A **70**, 022510 (2004).

[76] T. Pohl, H. R. Sadeghpour, Y. Nagata, and Y. Yamazaki, Phys. Rev. Lett. **97**, 213001 (2006).

[77] C. Taylor, J. Zhang, and F. Robicheaux, J. Phys. B: At. Mol. Opt. Phys. **39**, 4945 (2006).

[78] H. K. Chung, M. Chen, W. Morgan, Y. Ralchenko, and R. Lee, High Energy Density Phys. **1**, 3 (2005).

[79] M. Gryziński, Phys. Rev. **138**, A336 (1965).

[80] G. I. Budker and A. N. Skrinskǐ, Sov. Phys. Usp. **21**, 277 (1978).

[81] A. Müller and A. Wolf, Hyperfine Interact. **109**, 233 (1997).

[82] M. H. Holzscheiter, M. Charlton, and M. M. Nieto, Phys. Rep. **402**, 1 (2004).

[83] I. Meshkov and A. Skrinsky, Nucl. Instrum. Methods A **379**, 41 (1996).

[84] H. A. Bethe, and E. E. Salpeter, *Quantum Mechanics of One- and Two-Electron Atoms* (Plenum, New York, 1977).

[85] M. C. Fujiwara, M. Amoretti, C. Amsler, G. Bonomi, A. Bouchta, P. D. Bowe, C. Canali, C. Carraro, C. L. Cesar, M. Charlton, M. Doser, A. Fontana, R. Funakoshi, P. Genova, J. S. Hangst, R. S. Hayano, L. V. Jørgensen, A. Kellerbauer, V. Lagomarsino, R. Landua *et al.* (ATHENA Collaboration) Phys. Rev. Lett. **101**, 053401 (2008).

[86] U. Schramm *et al.* Phys. Rev. Lett. **67**, 22 (1991).

[87] F. B. Yousif, P. VanderDonk, Z. Kucherovsky, J. Reis, E. Brannen, J. B. A. Mitchell, and T. J. Morgan, Phys. Rev. Lett. **67**, 26 (1991).

[88] A. Wolf, Hyperfine Interact. **76**, 189 (1993).

[89] V. S. Melezhik, Hyperfine Interact. **193**, 329 (2009).

[90] I. I. Fabrikant and H. B. Ambalampitiya, Phys. Rev. A **101**, 053401 (2020).

[91] P. Blatt, Hyperfine Interact. **44**, 295 (1989).

[92] M. Amoretti, C. Amsler, G. Bonomi, P. D. Bowe, C. Canali, C. Carraro, C. L. Cesar, M. Charlton, A. M. Ejsing, A. Fontana, M. C. Fujiwara, R. Funakoshi, P. Geova, J. S. Hangst, R. S. Hayano, V. Jogensen, A. Kellerbauer, V. Lagomarsino, E. LodiRizzini, M. Macri, N. Madsen, G. Manuzio, D. Mitchard, P. Montagna, L. G. C. Posada, H. Pruys, C. Regenfus, A. Rotondi, H. H. Telle, G. Trestera, D. P. VanderWerf, A. Variola, L. Venturelli, Y. Yamazaki, and N. Zurlo (ATHENA Collaboration), Phys. Rev. Lett. **97**, 213401 (2006).

[93] J. W. Humberston, M. Charlton, F. M. Jacobson, and B. I. Deutch, J. Phys. B: At. Mol. Phys. **20**, L25 (1987).

[94] M. Charlton, Phys. Lett. A **143**, 143 (1990).

[95] B. I. Deutch, M. Charlton, M. H. Holzscheiter, P. Hvelplund, L. V. Jørgensen, H. Knudsen, G. Laricchia, J. P. Merrison, and M. R. Poulsen, Hyperfine Interact. **76**, 151 (1993).

[96] J. P. Merrison, H. Bluhme, J. Chevallier, B. I. Deutch, P. Hvelplund, L. V. Jørgensen, H. Knudsen, M. R. Poulsen, and M. Charlton, Phys. Rev. Lett. **78**, 2728 (1997).

[97] D. B. Cassidy, Eur. Phys. J. D **72**, 53 (2018).

[98] C. H. Storry, A. Speck, D. LeSage, N. Guise, G. Gabrielse, D. Grzonka, W. Oelert, G. Schepers, T. Sefzick, H. Pittner, M. Herrmann, J. Walz, T. W. Hansch, D. Comeau, and E. A. Hessels (ATRAP Collaboration), Phys. Rev. Lett. **93**, 263401 (2004)

[99] E. A. Hessels, D. M. Homan, and M. J. Cavagnero, Phys. Rev. A **57**, 1668 (1998).

[100] J. W. Humberston, P. V. Reeth, M. S. T. Watts, and W. E. Meyerhof, J. Phys. B: At. Mol. Opt. Phys. **30**, 2477 (1997).

[101] A. S. Kadyrov, C. M. Rawlins, A. T. Stelbovics, I. Bray, and M. Charlton, Phys. Rev. Lett. **114**, 183201 (2015).

[102] C. M. Rawlins, A. S. Kadyrov, A. T. Stelbovics, I. Bray, and M. Charlton, Phys. Rev. A **93**, 012709 (2016).

[103] I. I. Fabrikant, A. S. Kadyrov, I. Bray, and M. Charlton, J. Phys. B: At. Mol. Opt. Phys. **50**, 134001 (2017).

[104] A. S. Kadyrov, I. Bray, M. Charlton, and I. I. Fabrikant, Nat. Commun. **8**, 1544 (2017).

[105] A. S. Kadyrov, C. M. Rawlins, M. Charlton, I. I. Fabrikant, and I. Bray, Hyperfine Interact. **239**, 42 (2018).

[106] D. Krasnický, R. Caravita, C. Canali, and G. Testera, Phys. Rev. A **94**, 022714 (2016).

[107] D. Krasnicky, G. Testera, and N. Zurlo, J. Phys. B: At. Mol. Opt. Phys. **52**, 115202 (2019).

[108] D. Krasnický, G. Testera, and N. Zurlo, J. Phys. B: At. Mol. Opt. Phys. **53**, 239601(E) (2020).

[109] H. B. Ambalampitiya, D. V. Fursa, A. S. Kadyrov, I. Bray, and I. I. Fabrikant, J. Phys. B: At. Mol. Opt. Phys. **53**, 155201 (2020).

[110] M. Charlton, H. B. Ambalampitiya, I. I. Fabrikant, D. V. Fursa, A. S. Kadyrov, and I. Bray, Phys. Rev. A **104**, L060803 (2021).

[111] I. I. Fabrikant, J. Phys. B: At. Mol. Phys. **7**, 91 (1974).

[112] E. P. Wigner, Phys. Rev. **73**, 1002 (1948).

[113] M. Gailitis and R. Damburg, Proc. Phys. Soc. **82**, 192 (1963).

[114] C. M. Keating, and J. C. Straton, *Using Strong Laser Fields to Produce Antihydrogen Ions* (2018), https://pdxscholar.library.pdx.edu/open_access_etds/4519/.

[115] J. S. Vogel, AIP Conference Proc. **1655**, 020015 (2015).

[116] M. Stenrup, A. Larson, and N. Elander, Phys. Rev. A **79**, 012713 (2009).

[117] H. M. Hedberg, S. Nkambule, and A. Larson, J. Phys. B: At. Mol. Opt. Phys. **47**, 225206 (2014).

[118] S. M. Nkambule, N. Elander, A. Larson, J. Lecointre, and X. Urbain, Phys. Rev. A **93**, 032701 (2016).

[119] J. Hörnquist, P. Hedvall, A. Larson, and A. E. Orel, Phys. Rev. A **106**, 062821 (2022).

[120] S. Szucs, M. Karemera, M. Terao, and F. Brouillard, J. Phys. B: At. Mol. Phys. **17**, 1613 (1984).

[121] B. Peart and D. A. Hayton, J. Phys. B: At. Mol. Opt. Phys. **25**, 5109 (1992).

[122] J. Hörnquist and A. Larson (private communication).
[123] P. Pérez *et al.* (GBAR Collaboration), Hyperfine Interact. **233**, 21 (2015).
[124] P. Comini and P. A. Hervieux, New J. Phys. **15**, 095022 (2013).
[125] P. Comini and P. A. Hervieux, J. Phys.: Conf. Ser. **443**, 012007 (2013).
[126] P. Comini, P. A. Hervieux, and F. Biraben, Hyperfine Interact. **228**, 159 (2014).
[127] P. Comini, P. A. Hervieux, and K. Lévêque-Simon, New J. Phys. **23**, 029501 (2021).
[128] P. Froelich, T. Yamashita, Y. Kino, S. Jonsell, E. Hiyama, and K. Piszczatowski, Hyperfine Interact. **240**, 46 (2019).
[129] T. Yamashita, Y. Kino, E. Hiyama, S. Jonsell, and P. Froelich, New J. Phys. **23**, 012001 (2021).
[130] T. Yamashita, Y. Kino, E. Hiyama, S. Jonsell, and P. Froelich, Phys. Rev. A **105**, 052812 (2022).
[131] A. Jacob, C. Müller, and A. B. Voitkiv, Phys. Rev. A **104**, 032802 (2021).
[132] D. F. Dance, M. F. A. Harrison, R. D. Rundel, and A. C. H. Smith, Proc. Phys. Soc. **92**, 577 (1967).
[133] G. H. Dunn and B. Van Zyl, Phys. Rev. **154**, 40 (1967).
[134] J. M. Peek, Phys. Rev. A **10**, 539 (1974).
[135] M. C. Zammit, D. V. Fursa, and I. Bray, Phys. Rev. A **88**, 062709 (2013).
[136] M. C. Zammit, D. V. Fursa, and I. Bray, Phys. Rev. A **90**, 022711 (2014).
[137] L. H. Scarlett, M. C. Zammit, D. V. Fursa, and I. Bray, Phys. Rev. A **96**, 022706 (2017).
[138] T. Takagi, Phys. Scr. **T96**, 52 (2002).
[139] M. Stroe and M. Fifirig, J. Phys. B: At. Mol. Opt. Phys. **42**, 205203 (2009).
[140] M. Fifirig and M. Stroe, J. Phys. B: At. Mol. Opt. Phys. **44**, 085202 (2011).
[141] K. Chakrabarti, Backodissa-D. R. Kiminou, N. Pop, J. Z. Mezei, O. Motapon, F. Lique, O. Dulieu, A. Wolf, and I. F. Schneider, Phys. Rev. A **87**, 022702 (2013).
[142] R. K. Janev, D. Reiter, and U. Samm, Collision processes in low-temperature hydrogen plasmas, Technical Report, Forschungszentrum Juelich GmbH (Germany). Inst. fuer Plasmaphysik, EURATOM Association, Trilateral Euregio Cluster (2003), https://www.eirene.de/Documentation/report_4105.pdf.
[143] M. C. Zammit, J. S. Savage, J. Colgan, D. V. Fursa, D. P. Kilcrease, I. Bray, C. J. Fontes, P. Hakel, and E. Timmermans, Astrophys. J. **851**, 64 (2017).
[144] N. Mori, R. Utamuratov, L. Scarlett, D. Fursa, A. Kadyrov, I. Bray, and M. Zammit, J. Phys. B **53**, 015203 (2019).
[145] D. R. Bates, U. Ípik and G. Poots, Proc. Phys. Soc. A **66**, 1113 (1953).
[146] D. R. Bates, and U. Ípik, J. Phys. B: At. Mol. Phys. **1**, 543 (1968).
[147] D. J. Haxton, Phys. Rev. A **88**, 013415 (2013).
[148] A. Singor, L. H. Scarlett, M. C. Zammit, I. Bray, and D. V. Fursa, Astrophys. J. Suppl. Ser. **269**, 19 (2023).
[149] X. Urbain, A. Cornet, F. Brouillard, and A. Giusti-Suzor, Phys. Rev. Lett. **66**, 1685 (1991).
[150] J. M. C. Rawlings, J. E. Drew, and M. J. Barlow, Mon. Not. R. Astron. Soc. **265**, 968 (1993).
[151] J. Hörnquist, P. Hedvall, A. E. Orel, and A. Larson, Phys. Rev. A **108**, 052811 (2023).
[152] F. Brouillard and X. Urbain, Phys. Scr. **T96**, 86 (2002).
[153] D. Nehari, F. Brouillard, J. Jureta, and X. Urbain, J. Phys. B: At. Mol. Opt. Phys. **35**, 4733 (2002).
[154] R. C. Forrey, S. Jonsell, A. Saenz, P. Froelich, and A. Dalgarno, Phys. Rev. A **67**, 040701 (2003).
[155] A. Bohr, A. Blickle, S. Paolini, L. Ohlinger, and R. C. Forrey, Phys. Rev. A **85**, 042710 (2012).
[156] J. Taylor, B. Vargo, D. Hoffman, T. J. Price, and R. C. Forrey, Phys. Rev. A **109**, 052816 (2024).
[157] J. Hörnquist, A. E. Orel, and A. Larson, Phys. Rev. A **109**, 052806 (2024).
[158] G. Poulaert *et al.* J. Phys. B: At. Mol. Phys. **11**, L671 (1978).
[159] X. Urbain, A. Giusti-Suzor, D. Fussen, and C. Kubach, J. Phys. B: At. Mol. Phys. **19**, L273 (1986).
[160] W. B. Latter and J. H. Black, Astrophys. J. **372**, 161 (1991).
[161] M. C. Zammit, J. S. Savage, D. V. Fursa, and I. Bray, Phys. Rev. Lett. **116**, 233201 (2016).
[162] M. C. Zammit, J. S. Savage, D. V. Fursa, and I. Bray, Phys. Rev. A **95**, 022708 (2017).
[163] L. H. Scarlett, J. K. Tapley, D. V. Fursa, M. C. Zammit, J. S. Savage, and I. Bray, Phys. Rev. A **96**, 062708 (2017)
[164] L. H. Scarlett, J. K. Tapley, D. V. Fursa, M. C. Zammit, J. S. Savage, and I. Bray, Eur. Phys. J. D **72**, 34 (2018)
[165] L. H. Scarlett, J. S. Savage, D. V. Fursa, I. Bray, and M. C. Zammit, Eur. Phys. J. D **74**, 36 (2020).
[166] L. H. Scarlett, D. V. Fursa, J. Knol, M. C. Zammit, and I. Bray, Phys. Rev. A **103**, L020801 (2021).
[167] M. Zawadzki, R. Wright, G. Dolmat, M. F. Martin, L. Hargreaves, D. V. Fursa, M. C. Zammit, L. H. Scarlett, J. K. Tapley, J. S. Savage, I. Bray, and M. A. Khakoo, Phys. Rev. A **97**, 050702 (2018).
[168] T. Meltzer, J. Tennyson, Z. Mašín, M. C. Zammit, L. H. Scarlett, D. V. Fursa, and I. Bray, J. Phys. B: At. Mol. Opt. Phys. **53**, 145204 (2020).
[169] L. H. Scarlett, D. V. Fursa, M. C. Zammit, I. Bray, Y. Ralchenko, and K. D. Davie, At. Data Nucl. Data Tables **137**, 101361 (2021).
[170] L. H. Scarlett, D. V. Fursa, M. C. Zammit, I. Bray, and Y. Ralchenko, At. Data Nucl. Data Tables **139**, 101403 (2021).
[171] T. Sharp, At. Data Nucl. Data Tables **2**, 119 (1970).
[172] Z. Karpas, V. Anicich, and W. T. Huntress, J. Chem. Phys. **70**, 2877 (1979).
[173] S. V. ONeil and W. P. Reinhardt, J. Chem. Phys. **69**, 2126 (1978).
[174] M. S. Pindzola, F. Robicheaux, J. P. Colgan, M. C. Witthoeft, and J. A. Ludlow, Phys. Rev. A **70**, 032705 (2004).
[175] R. Schuch, D. Belkic, E. Justiniano, W. Zong, and H. Gao, Hyperfine Interact. **108**, 195 (1997).
[176] A. S. Kheifets and I. Bray, Phys. Rev. A **58**, 4501 (1998).

Correction: Table II was placed incorrectly during the production process and now appears in the appropriate location. Citations in text have also been adjusted.